DEUTSCHE BUNDESBANK EUROSYSTEM

Discussion Paper

Deutsche Bundesbank
No 34/2026

What volatility reveals: Agnostic identification of exchange rate and treasury-market dynamics in inconvenient times

Lucas ter Steege
(Deutsche Bundesbank)

Sofia Velasco
(Banco de España)

Discussion Papers represent the authors' personal opinions and do not necessarily reflect the views of the Deutsche Bundesbank or the Eurosystem.

Editorial Board: Daniel Foos
Stephan Jank
Thomas Kick
Martin Kliem
Malte Knüppel
Christoph Memmel
Hannah Paule-Paludkiewicz

Deutsche Bundesbank, Wilhelm-Epstein-Straße 14, 60431 Frankfurt am Main,
Postfach 10 06 02, 60006 Frankfurt am Main

Tel +49 69 9566-0

Please address all orders in writing to: Deutsche Bundesbank, Press and Public Relations Division, at the above address or via email: www.bundesbank.de/contact

Internet http://www.bundesbank.de

Reproduction permitted only if source is stated.

DOI https://doi.org/10.71734/DP-2026-34
ISBN 978-3-98848-093-4
ISSN 2941-7503

What Volatility Reveals: Agnostic Identification of Exchange Rate and Treasury-Market Dynamics in Inconvenient Times*

Lucas ter Steege Sofia Velasco †
Deutsche Bundesbank Banco de España

August 19, 2026

Abstract

This paper studies the financial-market transmission of the April 2025 U.S. tariff announcements, with a particular focus on the unusual combination of dollar depreciation and rising long-term U.S. Treasury yields. We ask whether the market reaction can be understood as the propagation of a single tariff-announcement shock or instead reflects the interaction of distinct macro-financial disturbances. To address this question, we exploit time-varying volatility and non-Gaussian excess kurtosis in structural shocks to recover macro-financial forces without imposing event-based restrictions or exclusion assumptions. Our results show that the initial market reaction is consistent with a conventional safe-haven shock, but this mechanism cannot account for the subsequent joint behaviour of exchange rates and long-term U.S. Treasury yields. Instead, different segments of financial markets are dominated by distinct orthogonal shocks associated with safe-haven demand, confidence in U.S. institutions, Treasury-market intermediation, and changes in the convenience value of dollar-denominated safe assets.

Keywords: Exchange rates; Treasury yields; Risk premia; Trade policy shocks; Safe-haven dynamics; Heteroskedastic identification; Financial spillovers
JEL Codes: F31; F41; G14; E44; C32

*The views expressed in this paper are those of the authors and do not necessarily reflect the views of the Deutsche Bundesbank, Banco de España, or the Eurosystem. We would like to thank without endorsement Benjamin Born, Marek Jarocinski, Maximilian Konradt, Elmar Mertens, seminar participants at Banco de España, Deutsche Bundesbank and European Central Bank (IPA Economic Meeting), and conference participants at the Third International Conference on the Climate-Macro-Finance Interface (SAFE, RCEA) and at the 2026 Second WIRE Annual Workshop for useful comments and suggestions.
†lucas.ter.steege@bundesbank.de sofia.velasco@bde.es

1 Introduction

On 2 April 2025, the U.S. administration announced a broad package of tariffs, proposing one of the largest increases in trade barriers in recent history.[1] The announcement triggered large movements across global financial markets. While some of these reactions were consistent with a rise in uncertainty-equity prices declined and volatility increased-others were more difficult to reconcile with conventional safe-haven dynamics. In the weeks that followed, the U.S. dollar depreciated against major currencies while long-term U.S. Treasury yields rose sharply. These unusual co-movements are particularly striking given the privileged role of the U.S. dollar and U.S. Treasuries in the international monetary system. Traditionally, episodes of heightened uncertainty have been associated with dollar appreciation and lower Treasury yields. The 2025 tariff episode therefore raises the possibility that exchange-rate and Treasury-market dynamics were driven by forces extending beyond a conventional tariff-announcement shock, potentially reflecting changes in the convenience value attached to dollar assets and U.S. Treasuries.

The privileged international role of the U.S. dollar is reflected in several interconnected features of the international monetary system. Dollar-denominated safe assets command unusually low expected returns because investors value their liquidity, safety, and collateral services (Du, Im, and Schreger, 2018; Krishnamurthy and Lustig, 2019; Payne and Szoke, 2025). Dollar liabilities also occupy a dominant position in global funding markets and international balance sheets (Cetorelli and Goldberg, 2012; Shin, 2012; Ivashina, Scharfstein, and Stein, 2015; Bruno and Shin, 2017; Maggiori, Neiman, and Schreger, 2020). Theoretical work further emphasizes that the dollar's role as a unit of account in trade invoicing is complementary to its role as a safe store of value, helping to sustain its dominance in both trade and global finance (Gopinath and Stein, 2021). During episodes of heightened global uncertainty, investors have historically sought both dollar liquidity and U.S. Treasuries, resulting in a joint appreciation of the dollar and a decline in Treasury yields (Jiang, Krishnamurthy, and Lustig, 2018, 2021). Together, these features underpin the international role of the dollar and the notion of U.S. exorbitant privilege (Gourinchas and Rey, 2007, 2022; Jiang, Richmond, and Zhang, 2024). Recent work further argues that the dollar exchange rate itself reflects the convenience value attached to dollar-denominated safe assets, linking movements in exchange rates directly to changes in the scarcity of dollar safe assets and the Treasury basis (Jiang et al., 2021; Jiang, Krishnamurthy, and Lustig, 2024; Gopinath and Stein, 2021). Against this backdrop, the market developments following the April 2025 tariff announcement raise the possibility that these different dimensions of international privilege did not move in tandem.

Aware that this episode represents only a snapshot, we view it as a rare opportunity to study forces that are often difficult to observe directly. The tariff announcement provides a focal point, but the subsequent dollar depreciation and rise in long-term Treasury yields may reflect several overlapping disturbances rather than a tariff shock alone. We therefore exploit variation in volatility over nearly two decades to recover macro-financial shocks without imposing sign restrictions, event-specific assumptions, or exclusion restrictions. We subsequently assign an economic interpretation to the recovered shocks

[1] The measures, widely referred to as "Liberation Day", were implemented through Executive Order No. 14257 and included a 10% baseline tariff on imports from more than 180 countries together with additional reciprocal tariffs linked to bilateral trade imbalances.

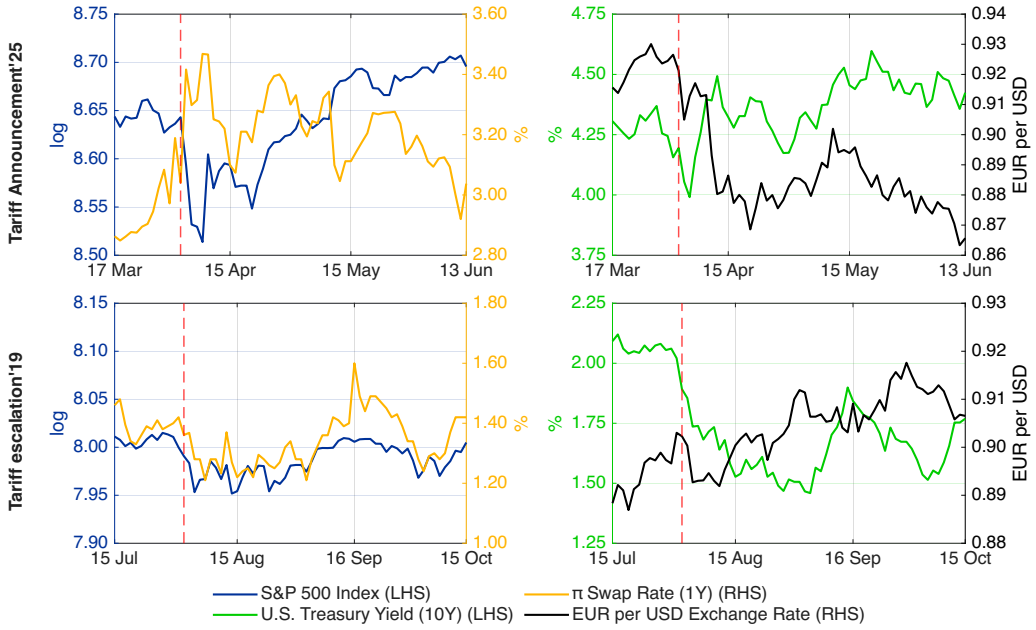
based on their empirical transmission patterns together with the mechanisms emphasized in the literature. Our agnostic statistical identification strategy is particularly valuable because several recent theories can account for similar reduced-form movements in exchange rates and Treasury yields, yet attribute them to distinct structural mechanisms, including shifts in safe-haven demand, confidence in U.S. institutions, Treasury-market intermediation, and changes in the convenience value attached to dollar-denominated safe assets. Distinguishing between these mechanisms is economically important because similar asset-price movements need not imply a common underlying shock. Whether the episode reflects a single disturbance or several distinct structural shocks has fundamentally different implications for how we interpret the role of the dollar, U.S. Treasuries, and the transmission of global financial stress. The resulting impulse responses allow us to assign an economic interpretation to the statistically identified shocks, while the historical decomposition shows that these mechanisms are jointly required to explain the 2025 episode. A conventional *Safe-Haven shock* captures the familiar flight-to-safety pattern of weaker equity prices, dollar appreciation, and lower Treasury yields, accounting for the broad risk-off component of the episode, particularly in equity markets. However, it cannot explain the joint dollar depreciation and rise in long-term Treasury yields observed after the tariff announcement. Instead, the dollar depreciation and rise in long-term Treasury yields are primarily associated with a broad repricing of U.S. dollar assets consistent with a deterioration in U.S. institutional credibility, while a distinct *Treasury Market Intermediation shock* accounts for the deterioration in swap spreads and Treasury Convenience. Taken together, the evidence suggests that the April 2025 episode did not reflect the breakdown of a single safe-haven mechanism. Rather, it revealed distinct dimensions of U.S. international privilege that are ordinarily difficult to disentangle empirically.

Interpreting these developments poses a challenge for existing frameworks of exchange-rate and Treasury-market determination. The joint depreciation of the dollar and increase in long-term Treasury yields following the tariff announcement contrasts sharply with the behaviour typically observed during episodes of heightened uncertainty. This combination is difficult to reconcile with canonical safe-haven dynamics, under which adverse shocks such as a unilateral increase in trade barriers are generally associated with dollar appreciation and declining Treasury yields. This pattern is well documented in the literature on global risk shocks, safe-haven currencies, and the global financial cycle, where increases in global risk premia systematically trigger a flight into dollar-denominated safe assets and U.S. Treasuries (Hossfeld and MacDonald, 2015; Rey, 2015; Jiang et al., 2018, 2021; Georgiadis, Müller, and Schumann, 2024; Müller, Georgiadis, and Schumann, 2023). Standard open-economy theory predicts that tariffs imposed by a dominant-currency country should appreciate the domestic currency through expenditure-switching effects, particularly under dominant-currency pricing (Gopinath, Boz, Casas, Díez, Gourinchas, and Plagborg-Møller, 2020). Consistent with these predictions, earlier U.S. tariff episodes, including those of 2018–2019, were associated with dollar appreciation (Furceri, Hannan, Ostry, and Rose, 2018; Jeanne and Son, 2024).

Importantly, the market reaction observed in the days and weeks following the April 2025 tariff announcement need not have been generated by the announcement alone. The emerging literature offers several competing interpretations. Pinter, Smets, and Üslü (2025) show that tariff-announcement shocks explain much of the initial reaction in equities, volatility, commodity prices and short-term inflation compensation, but account

for little of the persistent dollar depreciation and movements in long-term government bond yields, which they attribute to orthogonal shocks associated with Treasury-market dysfunction. Frankovic and Karau (2026) find that shocks to "U.S. confidence" account for much of the gold and exchange rate movements around the April 2025 event, as well as some of the observed stock market movements. Ostry, Lloyd, and Corsetti (2025) argue that once expected foreign retaliation is taken into account, the exchange-rate response is considerably less puzzling than the behaviour of long-term Treasury yields. Other contributions instead emphasize portfolio rebalancing away from U.S. assets, changes in foreign-investor hedging demand, or a reassessment of the convenience value attached to dollar-denominated safe assets and Treasury markets (Du, Keerati, and Schreger, 2026). These competing interpretations imply similar movements in observed asset prices while reflecting fundamentally different underlying structural disturbances. Rather than identifying a tariff-specific shock, we therefore recover a set of macro-financial disturbances over the full sample and examine their contribution to the dynamics observed during the 2025 episode.

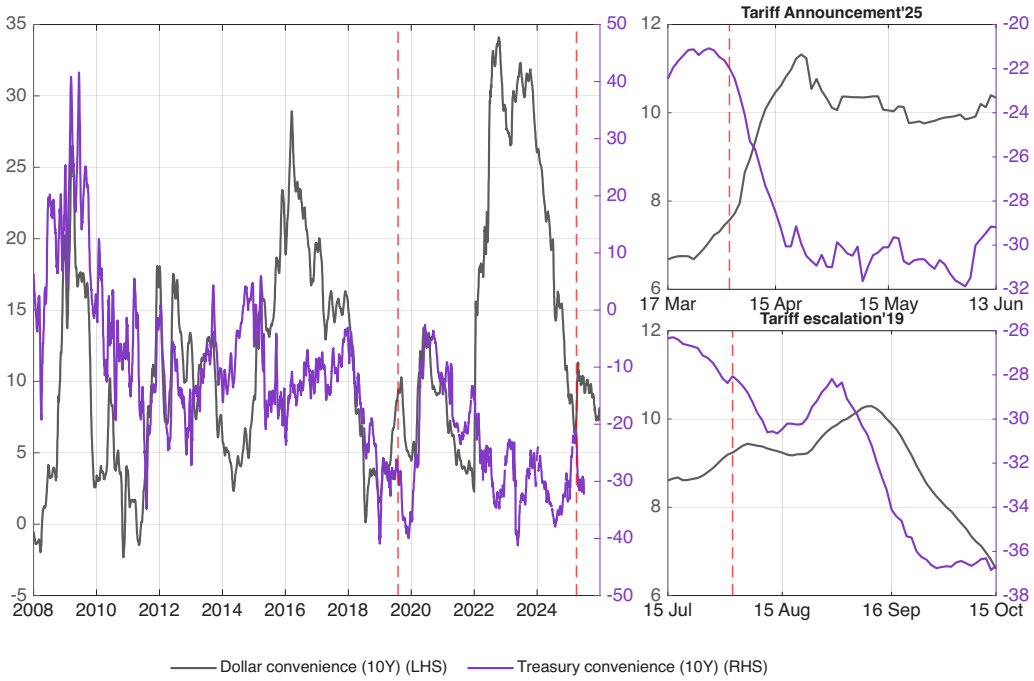
Figure 1 compares financial-market developments following the 2025 tariff announcement with those observed during the August 2019 tariff escalation. The comparison is informative because both episodes were associated with a deterioration in investor sentiment, yet the subsequent behaviour of key financial variables differed markedly. In both cases, equity prices declined on impact. However, unlike in 2019, the 2025 episode was characterised by a persistent depreciation of the U.S. dollar against the euro despite weaker equity markets. At the same time, long-term U.S. Treasury yields increased after the initial impact and remained elevated, while inflation compensation, measured by the one-year inflation swap rate, rose substantially. Relative to the benchmarks discussed above, this combination suggests that the 2025 episode reflected additional forces beyond a conventional tariff or global-risk shock.



Notes: The figure compares four financial variables around the 2025 tariff announcements (15 March–13 June 2025) and the August 2019 tariff escalation (15 July–15 October 2019). The S&P 500 index is reported in logs, while the EUR per USD exchange rate is reported in levels. The 1-year inflation swap rate and the 10-year U.S. Treasury yield are reported in percent. The 1-year inflation swap rate corresponds to the fixed rate exchanged against realized U.S. CPI inflation over a one-year horizon and serves as a market-based measure of short-term inflation compensation. The 10-year Treasury yield is the market yield on U.S. Treasury securities at constant 10-year maturity, quoted on an investment basis. The EUR per USD exchange rate is expressed as euros per U.S. dollar, so an increase denotes a dollar appreciation. Vertical dashed lines denote major tariff-announcement dates: 2 April 2025 (top row); 1 August 2019 (bottom row).

Figure 1: Financial Market Developments around Major U.S. Tariff Announcements

Recent work increasingly views U.S. international privilege as comprising several distinct but related dimensions. In particular, the literature distinguishes between global demand for dollar-denominated safe assets, Treasury-market functioning, and the convenience value attached specifically to U.S. Treasuries. Although these mechanisms can generate similar movements in exchange rates and bond yields, they reflect different underlying economic forces and have become central to interpreting recent episodes of market stress.



Notes: The figure compares two long-horizon convenience-yield measures over the estimation sample (2 January 2008–15 May 2025) and around two major tariff episodes. Dollar Convenience (10Y) measures the convenience value attached to holding long-term dollar-denominated safe assets after hedging exchange-rate risk (Du et al., 2026). Treasury Convenience (10Y) isolates the additional convenience value attached specifically to U.S. Treasury securities relative to other G10 government bonds (Du et al., 2018, 2026). The left panel reports both series over the full estimation sample. The right panels compare their behaviour around the April 2025 tariff announcement (15 March–13 June 2025) and the August 2019 tariff escalation (15 July–15 October 2019). Both series are expressed in basis points. Vertical dashed lines denote the major tariff-announcement dates: 2 April 2025 and 1 August 2019.

Figure 2: Dollar and Treasury Convenience around Major U.S. Tariff Announcements

Following the Global Financial Crisis, Treasury-market structure changed substantially. Regulatory reforms constrained dealer balance sheets while non-bank intermediaries assumed an increasingly important role in Treasury intermediation. The March 2020 Treasury-market turmoil exposed these structural vulnerabilities, demonstrating that Treasury-market functioning could deteriorate despite exceptionally strong global demand for dollar liquidity (Kashyap, Stein, Wallen, and Younger, 2025). Building on this evidence, Du et al. (2026) show that Dollar Convenience and Treasury Convenience have become increasingly distinct dimensions of U.S. international privilege, consistent with evidence that rising relative U.S. risk has been an important driver of the Treasury Convenience yield (Corsetti, Lloyd, Marin, and Ostry, 2026).

Figure 2 summarizes this evolution. The left panel shows that Dollar Convenience and Treasury Convenience broadly co-moved during the Global Financial Crisis and the European sovereign debt crisis but gradually diverged following the post-crisis restructuring of Treasury markets. The right panels compare the 2025 tariff episode with the 2019 tariff escalation. Unlike in 2019, the two measures moved in opposite directions during the 2025 episode, suggesting that investors reassessed different dimensions of U.S.

international privilege rather than uniformly reducing demand for U.S. safe assets.

This distinction motivates our empirical analysis. Rather than interpreting the 2025 episode as the realization of a single tariff or safe-haven shock, we allow separate structural disturbances to affect global safe-haven demand, confidence in U.S. institutions, and Treasury-market functioning. The historical decomposition subsequently shows that these mechanisms dominate different segments of financial markets, implying that the episode reflects the interaction of several orthogonal macro-financial shocks rather than the propagation of a single disturbance.

Our contribution relates to several strands of the literature. Structural models of tariff shocks impose economic mechanisms to discipline counterfactual outcomes (Kalemli-Özcan, Soylu, and Yildirim, 2025; Alessandria, Ding, Khan, and Mix, 2025; Auclert, Rognlie, and Straub, 2025; Rodríguez-Clare, Ulate, and Vasquez, 2025), but their implications for asset prices depend on assumptions about monetary policy, expectations, risk sharing, and the currency in which trade is invoiced. Bianchi and Coulibaly (2025), for instance, show that the optimal monetary policy response to tariffs is expansionary and depreciates the exchange rate, underscoring how strongly the exchange-rate implications of a tariff shock hinge on the assumed policy reaction. Ignatenko, Lashkaripour, Macedoni, and Simonovska (2025) instead quantify the long-run economic impacts of the 2025 tariffs in a structural general-equilibrium trade model calibrated to 194 countries. High-frequency event studies instead focus on narrow windows around announcements, isolating immediate valuation effects but typically abstracting from multi-shock dynamics (Ostry et al., 2025).[2] A close empirical benchmark is Pinter et al. (2025), who show that tariff-announcement shocks account for much of the initial market reaction, while the subsequent joint dynamics of the dollar and government bond yields are less tightly linked to the announcement itself. We build on this setting but depart from event-based identification by exploiting time variation in second moments over the full sample. This allows for a multi-shock environment in which safe-haven demand, dollar-asset pricing, and Treasury-market intermediation can be separated empirically rather than attributed ex ante to a single announcement shock. Methodologically, our framework builds on the heteroskedasticity-based identification approach of Rigobon (2003) and subsequent contributions. Identification arises from time variation in second moments: changes in the relative volatility of structural shocks allow the structural impact matrix to be recovered without exclusion restrictions. While non-Gaussianity can provide an additional source of identification through higher-order moments (Lanne, Meitz, and Saikkonen, 2017; Jarocinski, 2024), in our baseline SV-t specification it plays a complementary role by improving empirical fit and capturing the excess kurtosis present in financial data. This paper makes three contributions. First, we provide evidence that the financial-market dynamics following the April 2025 tariff announcement cannot be understood as the propagation of a single tariff or safe-haven shock. Instead, our historical decomposition shows that different components of the financial-market response were driven by distinct macro-financial shocks, including conventional safe-haven demand, changes in confidence in U.S. institutions, and Treasury-market intermediation. Second, we demonstrate how heteroskedasticity-based identification can be used to recover these overlapping structural shocks without relying on sign restrictions, event windows, or exclusion restrictions. The empirical application

[2]See also Hartley and Rebucci (2025) and Cardani, Kühl, Peppel-Srebrny, and Strauch (2025) for related high-frequency evidence on the financial-market response to the April 2025 announcement.

illustrates how statistically identified shocks can subsequently be given an economic interpretation through their transmission patterns and historical contributions. Third, across two empirical applications, we show that structural inference is robust to alternative specifications of the shock distribution. The recovered impulse responses remain comparable across different ways of modelling heteroskedasticity and excess kurtosis, consistent with the idea that identification relies on sufficiently informative variation in second moments, excess kurtosis, or both, rather than on a particular parametric specification.

The remainder of the paper is organised as follows. Section 2 presents the empirical framework and identification strategy. Section 3 analyses the financial-market dynamics surrounding the 2025 tariff episode. Section 4 concludes.

2 Model

We consider a VAR model for N endogenous variables of order p:

$$y_t = b_0 + B_1 y_{t-1} + \ldots + B_p y_{t-p} + A^{-1}\epsilon_t \tag{1}$$

$$\epsilon_t|\omega_t \sim \mathcal{N}(0, \Omega_t), \quad \Omega_t = diag(\omega_{1,t}e^{h_{1,t}}, \ldots, \omega_{N,t}e^{h_{N,t}}) \tag{2}$$

$$\omega_{i,t} \sim \mathcal{IG}\left(\frac{\nu_i}{2}, \frac{\nu_i}{2}\right), \quad \nu_i > 0 \tag{3}$$

$$h_{i,t} = \rho_i h_{i,t-1} + v_{i,t}, \quad |\rho_i| < 1, \quad v_{i,t} \sim \mathcal{N}(0, \sigma_i^2) \tag{4}$$

$$h_{i,1} \sim \mathcal{N}\left(0, \frac{\sigma_i^2}{1-\rho_i^2}\right) \tag{5}$$

The model specifies each structural error $\epsilon_{i,t}$ as featuring both heavy tails as in Lanne et al. (2017), Brunnermeier, Palia, Sastry, and Sims (2021), or Kociecki, Matthes, and Piffer (2025), and a stationary stochastic volatility component as in Chan, Koop, and Yu (2024). Without the stochastic volatility component the structural errors would follow a Student-t distribution, where the assumption $\nu_i > 0$ is enforced via the prior. The impact matrix containing the contemporaneous effects of the structural shocks, A^{-1}, is assumed to be invertible but otherwise unrestricted. As in Chan et al. (2024) our model is order-invariant, meaning that our estimates of individual volatilities and/or heavy tailedness do not depend on the specific ordering of the endogenous variables.[3]

2.1 Estimation

We use Markov chain Monte Carlo (MCMC) methods to estimate the model because its posterior distribution is analytically intractable. Here we briefly outline the prior distributions and sampling steps; full details on the prior hyperparameters and Gibbs sampler are provided in Appendix A.3. Let $\Theta = (\alpha, \beta, \omega, \nu, \rho, \sigma^2, h)$ be the collection of parameters in the model. $\alpha = \text{vec}(A)$ contains the coefficients of the inverse impact matrix, β denotes the VAR slope coefficients and constants. The $NT \times 1$ vector ω contains the variance parameters related to the Student-t distribution, the $N \times 1$ vector ν collects

[3] A related approach to achieving order invariance is proposed by Arias, Rubio-Ramírez, Shin, and Waggoner (2026), who develop rotation-invariant time-varying SVARs identified with sign restrictions. Our model instead assumes a constant contemporaneous impact matrix and exploits heteroskedasticity for identification, a class of models explicitly excluded from their framework.

the respective degrees of freedom. Lastly, ρ, σ^2, and h collect the parameters related to the N stochastic volatility processes. Our prior assumes independence between the parameter blocks.

The Gibbs sampler cycles through the following steps, where θ denotes the set of parameters other than the ones being sampled in the respective steps:

1. $p(\alpha|y,\theta) = p(\alpha|y,\beta,\omega,h)$
2. $p(\beta|y,\theta) = p(\beta|y,\alpha,\omega,h)$
3. $p(\omega|y,\theta) = \prod_{i=1}^{N}\prod_{t=1}^{T} p(\omega_{i,t}|y,\alpha,\beta,\nu_i,h_{i,t})$
4. $p(\nu|y,\theta) = \prod_{i=1}^{N} p(\nu_i|\omega_i)$
5. $p(\sigma^2|y,\theta) = \prod_{i=1}^{N} p(\sigma_i^2|\rho_i,h_i)$
6. $p(\rho|y,\theta) = \prod_{i=1}^{N} p(\rho_i|\sigma_i^2,h_i)$
7. $p(h|y,\theta) = \prod_{i=1}^{N} p(h_i|y,\alpha,\beta,\omega_i,\rho_i,\sigma_i^2)$

To sample α we use the algorithm in Chan et al. (2024) who build on earlier work by Waggoner and Zha (1999) and Villani (2009). For the last step we use the auxiliary mixture sampler from Kim, Shephard, and Chib (1998). As noted in Del Negro and Primiceri (2015), it is important to sample the auxiliary mixture indicators before the log-volatilities are sampled to draw from the correct conditional posterior (see also Chan (2024)). In the spirit of Bertsche and Braun (2022) we remove the empirical mean from each draw for h_i during the posterior sampler which implicitly fixes the scale of the structural A matrix. We do so to avoid potential scaling issues in the posterior if no prior information on the scale of the structural shocks is supplied to the model. This is the standard mean-zero log-volatility normalization used in Chan and Hsiao (2014), needed because the level of h_i and the scale of the corresponding row of A are not separately identified without a prior on that scale. Most other steps of the sampler are standard, except for those related to ν_i and ρ_i. As these densities are univariate we use a Griddy-Gibbs step as in Ritter and Tanner (1992).

As is well known in this type of model, the order of the structural shocks and the columns of the impact matrix A^{-1} is arbitrary. Furthermore, it is always possible to flip the sign of a given column and the corresponding shock without changing the likelihood function of the model. Hence, a procedure is necessary to normalise the posterior draws to yield reliable inference. We combine the approaches by Kociecki et al. (2025) and Poworoznek, Anceschi, Ferrari, and Dunson (2021) to do so. Having obtained the desired number of draws from the posterior, we use the efficient approach by Kociecki et al. (2025) to choose the sign-permutation of a given draw that minimizes the Frobenius norm between the permutation and a reference matrix. Instead of using the maximum likelihood estimator as the reference matrix we determine the reference point from the posterior sample itself based on the impact matrix with median condition number, in line with Poworoznek et al. (2021). They suggest to use the condition number as it proxies unique information contained in the columns of the impact matrix draws, based on which we wish to normalise the draws. Choosing the median then ensures that one uses a

representative draw from the posterior. This is similar in spirit to choosing the maximum likelihood estimator as the reference point, provided that it is close to the posterior mode, which may not be the case in practice. Furthermore, the approach we use is much simpler to implement. We provide a detailed description in Appendix A.4.

2.2 Identification

In addition to being well suited to modelling financial time series, the model can be statistically identified when the structural shocks exhibit sufficient heteroskedasticity, excess kurtosis, or both. Specifically, Bertsche and Braun (2022) show that the model is fully identified if the shocks are mutually uncorrelated and $|\rho_i| \neq 0$ for $i = 1, \ldots, N-1$. A similar result obtains even if no heteroskedasticity is present but the shocks are independent and at most one has a Gaussian distribution. Below we investigate both features and indeed find that these identification results apply in our case. The intuition behind the identification result in the case of independent Student-t structural shocks is nicely illustrated in Jarocinski (2024), which applies to our model as well. When the shocks are Gaussian, the model can make use only of the first and second moments of the residual distribution. The classic identification problem then results from the fact that there are infinitely many ways to factor a given residual covariance matrix to produce an estimate for A^{-1} that the model cannot distinguish between, as all such factorizations are observationally equivalent. When the structural shocks have non-Gaussian distributions, however, excess kurtosis breaks this invariance. With a heavy-tailed shock distribution it sometimes happens that one shock obtains a large, outlying value while all other shocks obtain only small values. In this case the observed data are driven predominantly by one shock only, revealing its effects. This is similar in spirit to an event-study approach in which particular observations are known to be driven by specific forces only, which are thus identifiable from the observable data. The same intuition applies when identification arises from heteroskedasticity. Assume for simplicity the case of two structural shocks only, of which only one is heteroskedastic. The reason we can identify the shocks in this case is also the fact that the heteroskedastic shock will occasionally realize with a large value due to its inflated variance, thus being responsible for the bulk of the observed variation in this instance. A potential problem with this approach, however, is that identification is only statistical in nature, and the identified shocks may not carry economic meaning. To resolve this issue we inspect the impulse response functions of the model to attach economic meaning to the identified shocks.

These identification results, however, presume that the econometrician has correctly specified the process generating the heteroskedasticity or excess kurtosis, an assumption Bertsche and Braun (2022) themselves show, via simulation, is not essential: their SV-SVAR remains reliable even when the variance process is misspecified relative to the truth. Sims (2021) formalizes why such robustness should hold more generally: identification survives misspecified variance regimes because what matters is that relative shock variances vary sufficiently over the sample, not that the analyst's parametric model for that variation is correct. Two empirical applications in this paper show that our structural results are stable across specifications that rely on different identification channels, so that identification is not tied to a particular volatility specification but instead requires sufficiently informative variation in second moments, excess kurtosis, or both. First, in

the oil-market application of Appendix B, we replicate the benchmark results of Bertsche and Braun (2022) in a Bayesian framework under three alternative specifications of the variance dynamics, a t-Distribution model, an SV model, and an SV-t specification, and the estimated impulse responses closely match the frequentist benchmark across all three variants, with only minor quantitative differences. Second, in our main application to the 2025 tariff announcement, Appendix Figures C.8 and C.9 show that the impulse responses to the identified shocks are qualitatively similar across the SV, t-Distribution, and SV-t specifications, with somewhat larger quantitative differences under the t-Distribution model. Together, these two applications indicate that heteroskedastic identification is robust to the choice of variance specification in practice.

3 Financial Market Dynamics Around the 2025 Tariff Announcement

We analyse financial-market dynamics around the April 2025 tariff announcement using a VAR with stochastic volatility and Student-t innovations. Consistent with the identification strategy introduced above, structural shocks are identified via time-varying volatility and non-Gaussian excess kurtosis, without imposing sign restrictions, exclusion restrictions, or event-specific assumptions (Rigobon, 2003; Bertsche and Braun, 2022). Our empirical design does not isolate a tariff-specific structural shock. Instead, we estimate a set of macro-financial shocks over the full sample and use them to decompose asset-price movements during the April 2025 tariff episode. This approach allows us to assess whether the observed dynamics can be attributed to a single dominant disturbance or instead reflect the interaction of multiple underlying shocks, including those unrelated to the initial tariff announcement.

The analysis uses daily data spanning 2 January 2008 to 15 May 2025; the sample start is dictated by the availability of Dollar Convenience (10Y), the latest-starting endogenous series. The complete set of series is reported in Appendix Table C.1. The baseline information set captures broad macro-financial conditions. The S&P 500 and the VIX measure global risk sentiment, the EUR per USD exchange rate captures the external value of the dollar, and the one-year inflation swap rate summarizes market-based inflation expectations. We further add the three-month Treasury term premium from the Adrian–Crump–Moench (ACM) model (Adrian, Crump, and Moench, 2013), which captures compensation for near-term interest-rate risk and helps distinguish movements in short-maturity Treasury yields driven by risk compensation from those driven by changes in expected short rates. Together, these variables characterise the benchmark transmission of global risk, monetary-policy expectations, and exchange-rate dynamics emphasized in the literature on international macro-financial spillovers and recent tariff announcements (Habib and Stracca, 2012; Georgiadis et al., 2024; Pinter et al., 2025).

The second group of variables is designed to distinguish among competing explanations centered on the functioning of Treasury markets and the international role of dollar-denominated safe assets. The 10-year U.S. Treasury yield and the 10-year euro-area government bond yield capture the relative behaviour of long-term sovereign yields across the two currency areas. To measure Treasury-market intermediation more directly, we include the 10-year U.S. swap spread, which is closely linked to dealer balance-sheet ca-

pacity and limits to arbitrage (Boyarchenko, Gupta, Steele, and Yen, 2018; Kashyap et al., 2025; Adrian, Fleming, and Nikolaou, 2025). We further include two long-horizon covered interest parity (CIP) measures developed by Du et al. (2018, 2026). Dollar Convenience (10Y) measures the convenience value attached to holding long-term dollar-denominated safe assets after hedging exchange-rate risk, reflecting the non-pecuniary services that investors derive from their liquidity, collateral value, and reserve-currency status. Treasury Convenience (10Y) instead isolates the additional convenience value attached specifically to U.S. Treasuries relative to other G10 government bonds. Recent work emphasizes that these two dimensions of U.S. international privilege need not move together, implying that broader demand for dollar assets and Treasury-specific demand may evolve independently during periods of market stress (Du et al., 2026).

Taken together, these variables allow us to distinguish between conventional risk-off dynamics, Treasury-market intermediation shocks, and changes in the convenience value attached to dollar-denominated reserve assets. This distinction is particularly valuable because these mechanisms often imply similar movements in exchange rates and long-term yields while generating markedly different predictions for swap spreads, Treasury term premia, and long-horizon CIP deviations.

Before turning to the effects of the identified shocks, we examine empirical diagnostics consistent with the second- and higher-moment variation relevant for identification. The estimated volatility processes (Appendix Figure C.4) are highly persistent, with distinct idiosyncratic dynamics across equations that nonetheless comove during periods of acute market stress, most notably in early 2020 and again in March–April 2025. The posterior distributions of the Student-t degrees-of-freedom parameters further support the presence of non-Gaussianity. Trace plots for the normalised impact matrix (Appendix Figure C.5) show stable mixing, providing evidence that the sampler is well behaved.

3.1 Model specification

Before turning to the economic interpretation of the identified shocks, we justify our choice of the SV-t baseline against two nested alternatives: stochastic volatility only (SV) and a homoskedastic Student-t specification (t-Distribution). We compare the three specifications' out-of-sample predictive performance around the April 2025 tariff announcement, computing one-step-ahead predictive log scores following the methodology detailed in Appendix A.6. Table 1 reports the cumulative and average log scores over the evaluation window, together with the score attributed specifically to the tariff announcement date.

Over the full evaluation window, SV attains the best predictive performance, and the pure t-Distribution specification, which lacks any persistence in its volatility process, is the weakest of the three; SV-t falls in between, trailing SV but comfortably ahead of t-Distribution on both the cumulative and average score. On the single trading day that reflects the announcement, however, the ranking is not the same: both t-Distribution and SV-t score better than SV, with t-Distribution best of all, reflecting the value of fat tails during a sharp, discrete repricing episode. We therefore adopt SV-t as the baseline specification as a compromise between the two features highlighted by the forecasting exercise. SV provides the strongest predictive performance over the full evaluation window, whereas allowing for Student-t innovations improves the model's ability to accommodate the unusually sharp repricing around the announcement. The SV-t specification preserves most

Table 1: Out-of-sample predictive log scores

	Evaluation window		Tariff announcement
Model	Cumulative	Average	April 2025
t-Distribution	−243.370	−8.112	**−17.469**
SV	**−166.499**	**−5.550**	−18.706
SV-t	−174.235	−5.808	−18.066

Notes: Bold figures indicate the best-performing score in each column. The Cumulative and Average columns report the cumulative and average one-step-ahead log score over the 2 April–14 May 2025 evaluation window. The Tariff Announcement column reports the one-step-ahead log score for 3 April 2025, the first trading day to reflect the 2 April announcement (made after the market close), using information available through 2 April 2025. SV denotes stochastic volatility only; SV-t denotes stochastic volatility with Student-t innovations. Scores are negative throughout, so higher values (closer to zero) indicate better predictive performance.

of the full-window performance of SV while allowing transitory extreme observations to be absorbed without requiring them to generate persistent movements in latent volatility.

Although the log score favors SV over SV-t, we retain SV-t as our baseline because it guards against a potential oversmoothing tendency in persistent-volatility models: such models tend to explain an isolated outlier by raising volatility both before and after the event, a pattern more likely to reflect the persistence of the volatility process than a genuine feature of the data. The Student-t component instead allows the model to accommodate an isolated extreme observation without translating it into a persistent increase in latent volatility. Hartwig (2024) documents exactly this contrast: the stochastic-volatility-only specification models the onset of COVID-19 as a smooth rise in volatility that begins even before the pandemic, while adding a Student-t component eliminates this anticipatory pattern entirely.

Intuitively, SV-t inherits some of the flexibility of the Student-t component, namely additional robustness to sharp, discrete repricing episodes, without materially harming predictive performance relative to SV outside those episodes. Appendix Figure C.7 plots the daily and cumulative log scores of all three specifications over the full recursive evaluation window: SV and SV-t track each other almost exactly throughout, while the pure t-Distribution specification visibly and persistently falls behind from mid-April onward, underscoring that its full-sample weakness is not driven by a handful of dates but is pervasive across the window.

Importantly, and in line with the argument in Sims (2021) that sufficiently rich second-moment heterogeneity renders the likelihood informative for both model comparison and identification, this choice does not alter our structural identification. Appendix Figures C.8 and C.9 report the impulse responses to the identified shocks under all three specifications: differences are virtually negligible between SV and our SV-t baseline, the two best-performing specifications on the full-sample log score, while the t-Distribution model shows somewhat larger quantitative differences without altering the qualitative interpretation of the shocks.

3.2 Impulse responses

We now turn to the economic interpretation of the statistically identified shocks, characterising each shock through its combined effects on risk sentiment, exchange rates, Treasury yields, Treasury-market functioning, and the two dimensions of U.S. international privilege captured by Dollar Convenience and Treasury Convenience. This joint perspective is particularly informative because several competing explanations for the 2025 episode imply similar movements in exchange rates and long-term Treasury yields while differing markedly in their implications for Treasury-market intermediation and the convenience value attached to dollar-denominated safe assets. Figure 3 reports the impulse responses of four focal shocks that are most informative for understanding the dynamics surrounding the April 2025 tariff announcement. Their contributions to the episode are examined through the historical decomposition below. Following Jarocinski (2024), the effects are normalised using the empirical standard deviations of the structural shock series by multiplying the columns of the estimated impact matrices for each posterior draw by the estimated implied shock standard deviations. Appendix Figure C.6 reports the complete set of impulse responses.

The shock in the first row generates a decline in equity prices, a sharp increase in the VIX, an appreciation of the dollar, and lower U.S. Treasury yields. Short-term inflation compensation falls on impact, while euro-area long-term yields also decline, consistent with a broad-based flight into safe assets. Moreover, U.S. Treasury yields decline more strongly than euro-area yields, indicating a larger relative increase in demand for U.S. Treasuries than for euro-area government bonds. The resulting transmission closely matches the conventional risk-off pattern documented in the literature and captures the familiar safe-haven role of both the U.S. dollar and Treasuries. For these reasons we label this shock as a *Safe-Haven shock*. Treasury Convenience also declines modestly on impact. Although economically small, this response is consistent with the broader evidence in Du et al. (2026) that Treasury Convenience has weakened relative to other dimensions of dollar safe-asset demand.

For ease of presentation, we group the first two statistically identified structural shocks reported in Figure C.6 into a Safe-Haven shock, since they generate closely related risk-off dynamics. The impulse response reported in the first row of Figure 3 is obtained by summing their corresponding normalised impact responses, representing the impulse response to a simultaneous one-standard-deviation realization of both shocks, while the historical decomposition below analogously reports their combined contribution. The two shocks have very similar effects across variables, with the main differences arising in the exchange rate and euro-area bond yields. The first shock leads to an appreciation of the U.S. dollar, whereas the second generates an economically small depreciation and has little impact on euro-area bond yields. We consider this aggregation justified because, taken together, the two shocks account for virtually all of the movements in stock prices and volatility around the tariff announcements we study and, as we show below, their combined contribution to the exchange rate remains limited relative to the other shocks.

Besides its impact on the variables in the system, we can also gain further insights into this shock by inspecting the corresponding volatility processes in Appendix Figure C.4, namely the first two shown there. The first volatility process features notable spikes between October and December 2008 during the Great Financial Crisis, between

March and April 2020 at the onset of the global pandemic, and again in early April 2025. In all three episodes, stock prices plummeted, growth prospects deteriorated, and U.S. Treasury yields generally declined persistently. Consistent with this reading, the median normalized log-volatility of the first process has a correlation of 0.8628 with the (daily) VIX over the sample. The second volatility process captures the same episodes but is more erratic in nature. It therefore seems likely that the estimated effects of this shock are largely informed by episodes typically associated with safe-haven dynamics, lending further support to our economic interpretation.

The shock in the second row of Figure 3 is characterised by an immediate depreciation of the U.S. dollar together with higher long-term U.S. Treasury yields and a pronounced deterioration in Dollar Convenience. At the same time, Treasury Convenience and swap spreads respond little, suggesting that the shock does not primarily reflect disruptions to Treasury-market functioning. Instead, the combination of a weaker dollar, higher compensation for holding long-term U.S. assets, and a decline in Dollar Convenience is consistent with a broad repricing of U.S. dollar assets. Following the discussion in the introduction, we interpret this pattern as reflecting a deterioration in confidence in the institutional and policy environment underpinning the international role of the United States. We therefore label this shock the *U.S. Institutional Credibility shock*. As with the other labels, this terminology summarizes the shock's empirical transmission pattern rather than imposing or uniquely identifying a particular structural mechanism. Notably, this shock is also associated with a rise in one-year inflation compensation, significant at the 68% credible level (Figure 3). The joint occurrence of higher expected inflation and a weaker dollar is difficult to reconcile with a standard macroeconomic shock, which would typically be accompanied by dollar appreciation as markets price in a monetary policy response; while this broad repricing could in principle also reflect fiscal-risk premia or generic portfolio rebalancing, the specific context of the April 2025 tariff announcements makes a deterioration in institutional credibility a sensible interpretation.

The defining feature of the third shock is a pronounced deterioration in Treasury-market functioning. The shock generates a substantial decline in the swap spread, making it more negative, together with a marked decline in Treasury Convenience, while leaving Dollar Convenience largely unaffected. The resulting transmission is consistent with episodes in which dealers' risk-bearing capacity becomes impaired: as dealers approach internal risk limits, they reduce inventory, intermediate less aggressively, and require greater compensation for absorbing Treasury risk (Boyarchenko et al., 2018; Du et al., 2026). This mechanism is consistent with the intermediary-balance-sheet framework of Kashyap et al. (2025) and with dealer-level evidence in Li, Petrasek, and Tian (2026), who show that binding internal value-at-risk limits substantially reduce Treasury-market intermediation, as well as with the broader evidence on Treasury-market functioning and dealer capacity surveyed in Adrian et al. (2025). At the same time, the shock appears largely unrelated to broader macroeconomic conditions or changes in the economic outlook, as neither equity prices, volatility, nor inflation expectations respond significantly. We therefore interpret this disturbance as a *Treasury Market Intermediation shock*.

Finally, the fourth row depicts a *Safe-Asset Convenience shock*. Unlike the previous shocks, it is characterised primarily by a sizable increase in both Dollar Convenience and Treasury Convenience, while the remaining macro-financial variables respond only modestly, if at all. The shock therefore captures changes in the non-pecuniary value

that global investors attach to dollar-denominated safe assets, including their liquidity, collateral services, and reserve-currency role, rather than disruptions to Treasury-market functioning. This interpretation is consistent with recent work arguing that fluctuations in the convenience value of dollar-denominated safe assets constitute a distinct dimension of U.S. international privilege (Jiang et al., 2021; Du et al., 2026).

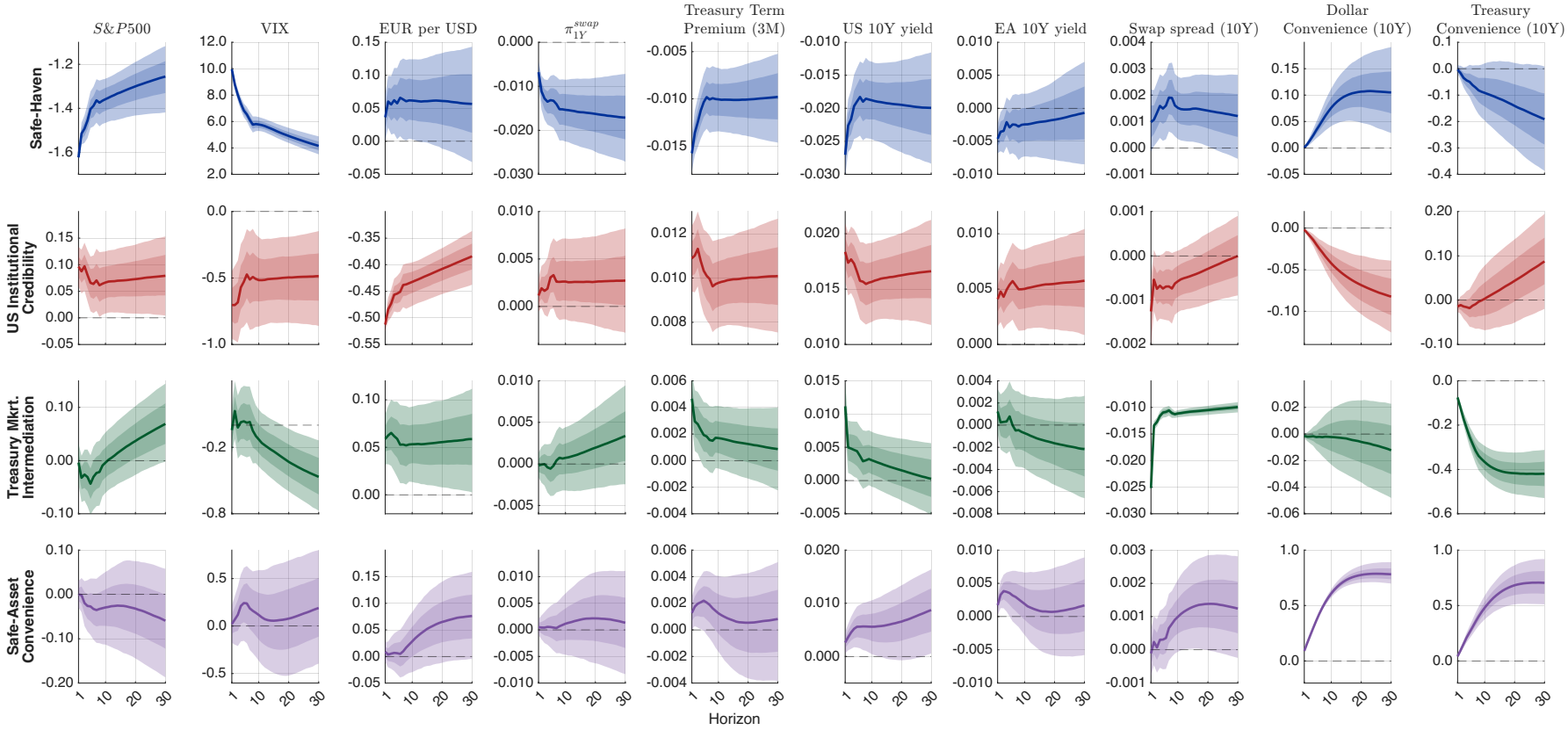


Figure 3: Impulse response functions

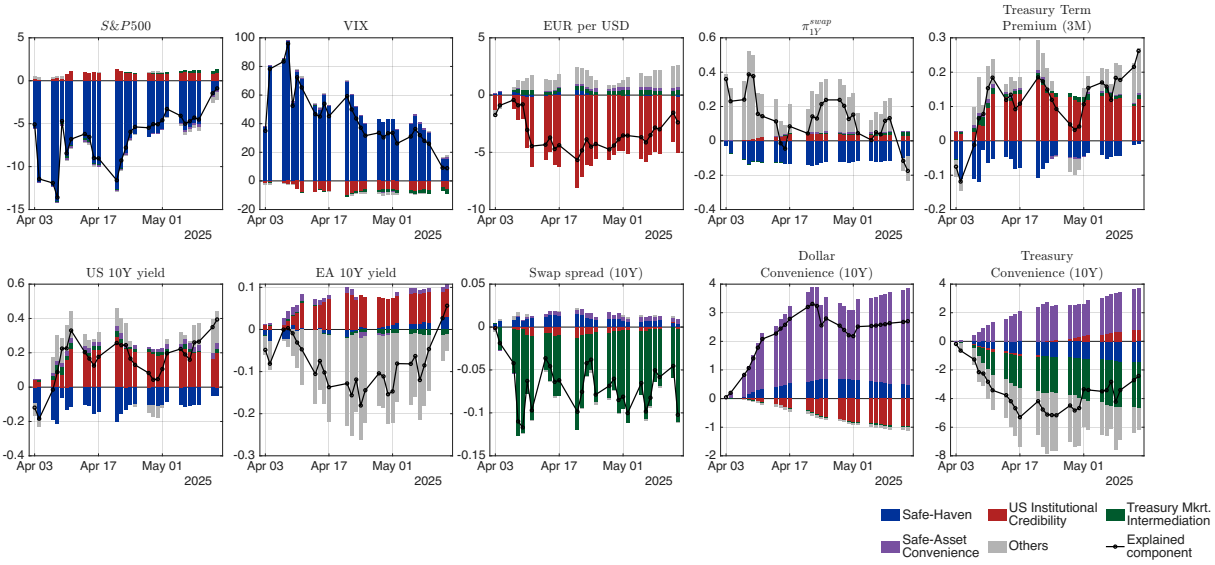
Notes: The figure reports impulse response functions over a 30-day horizon. Shaded areas denote 68% and 95% pointwise posterior credible intervals; the solid line is the posterior median. Rows show the *Safe-Haven shock* (shocks 1–2 combined; the reported response therefore corresponds to a simultaneous one-standard-deviation realization of both shocks, unlike the single-shock responses in the remaining rows), the *U.S. Institutional Credibility shock* (shock 3), the *Treasury Market Intermediation shock* (shock 8), and the *Safe-Asset Convenience shock* (shock 9).

3.3 Historical decompositions

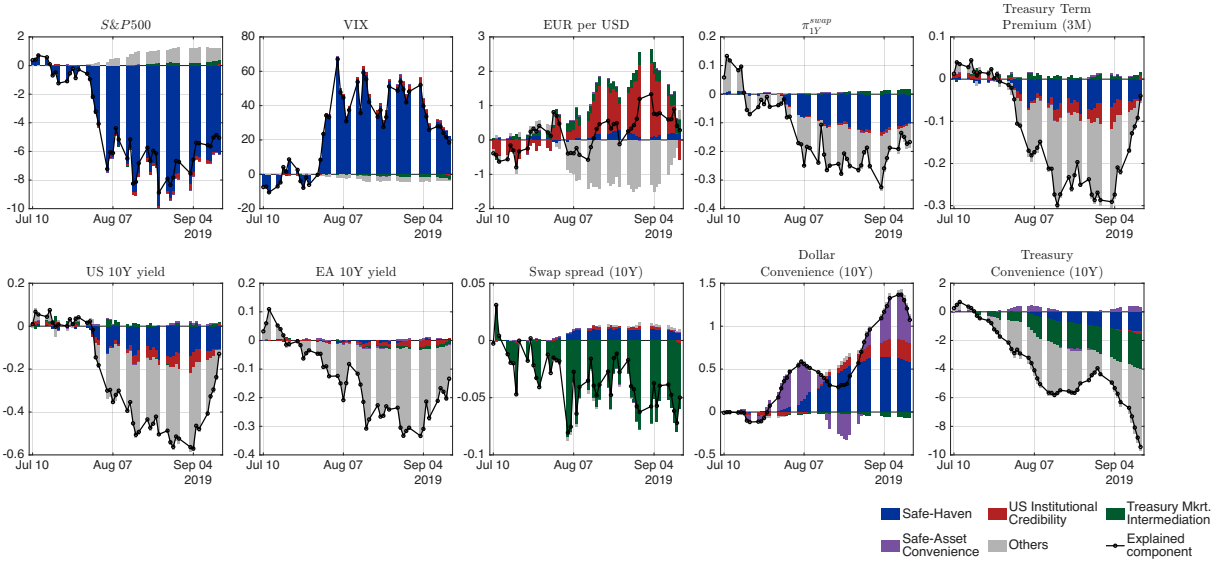
The impulse responses characterise how each statistically identified shock propagates through financial markets. An equally important question, however, is whether these shocks actually explain the behaviour of asset prices during the April 2025 tariff episode that motivates the analysis. Figure 4 therefore reports the historical decomposition, which quantifies the contribution of each structural shock to the observed evolution of financial markets. The historical decomposition evaluates the episode-specific relevance of our identified shocks: if the economic interpretation assigned to each shock is meaningful, that shock should account primarily for the financial variables whose impulse responses motivated its interpretation. The decomposition further lets us assess whether market dynamics can be explained by the propagation of a single estimated shock. Because our approach does not explicitly isolate a tariff-announcement shock, however, this exercise cannot rule out the possibility that the April 2025 announcement itself acted as a common catalyst for the several orthogonal shocks we identify. The evidence shows that different components of the financial-market response are dominated by different structural shocks, implying that the 2025 episode reflects the interaction of several orthogonal macro-financial forces rather than the propagation of a single disturbance.

The first result concerns the broad risk-off component of the episode. The decline in equity prices and the increase in implied volatility are explained predominantly by the *Safe-Haven shock*, consistent with the response identified in recent event-study evidence (Pinter et al., 2025). Thus, the decomposition confirms that conventional flight-to-safety forces account for the behaviour of equity markets. Furthermore, as noted in the introduction, the initial days of the April 2025 episode saw falling U.S. Treasury yields, as expected during a traditional safe-haven episode, and our first shock accounts for this pattern. The main empirical puzzle therefore does not lie in the equity-market response, but in the joint behaviour of exchange rates and fixed-income markets. The second result concerns the central empirical puzzle motivating the paper. Unlike equity markets, neither the depreciation of the dollar nor the increase in long-term Treasury yields following the initial impact is explained by the *Safe-Haven shock*. Instead, both movements are primarily associated with the *U.S. Institutional Credibility shock*, which accounts for the bulk of the rise in the three-month term premium and long-term Treasury yields and, strikingly, for nearly all of the observed exchange-rate depreciation. In this respect, our identified shock bears some resemblance to the "U.S. confidence" shock identified by Frankovic and Karau (2026). At the same time, our decomposition separates the response of equity markets from that of exchange rates and fixed-income markets, rather than attributing all of these movements to a single disturbance. The evidence therefore indicates that the unusual combination of a weaker dollar, higher long-term U.S. Treasury yields, and lower euro-area long-term yields cannot be interpreted as the propagation of a single tariff-announcement shock.

The third result concerns the distinct forces driving Dollar Convenience and Treasury Convenience. The decomposition shows that the two measures are driven by different structural shocks. Dollar Convenience is shaped mainly by the *U.S. Institutional Credibility shock* and the *Safe-Asset Convenience shock*. Treasury Convenience, by contrast, is driven primarily by the *Treasury Market Intermediation shock*, which also accounts for the deterioration in swap spreads. This close comovement is consistent with the inter-



(a) April 2025 Tariff Announcement



(b) August 2019 tariff escalation

Notes: Panel (a): historical decomposition for the April 2025 tariff window (2 April–14 May 2025). Panel (b): historical decomposition for the August 2019 tariff-escalation episode (9 July–15 September 2019). Stacked bars show the cumulative contributions of grouped statistically identified structural shocks; the black line is the explained component (deviation from the deterministic component). *Safe-Haven shock* = shocks 1–2; *U.S. Institutional Credibility shock* = shock 3; *Treasury Market Intermediation shock* = shock 8; *Safe-Asset Convenience shock* = shock 9; other shocks = shocks 4–7 and 10.

Figure 4: Historical decomposition around major U.S. tariff episodes

pretation of Du et al. (2026) that declines in Treasury Convenience increasingly reflect disruptions to Treasury-market intermediation and dealer balance-sheet capacity rather than changes in the broader convenience value of dollar-denominated safe assets. It also accords with the mechanism emphasized by Kashyap et al. (2025), whereby tighter intermediary balance-sheet constraints and reduced arbitrage capacity impair Treasury-market functioning.

Panel (b) of Figure 4 reports the corresponding decomposition for the August 2019 tariff escalation. The earlier episode is explained to a greater extent by the *Safe-Haven shock*, while the contributions of the *U.S. Institutional Credibility shock* and the *Treasury Market Intermediation shock* are more limited. Notably, the *Safe-Haven shock* also accounts for part, although not all, of the decline in the three-month term premium and long-term U.S. Treasury yields. The comparison suggests that the 2025 episode did not generate entirely new mechanisms. Rather, it amplified forces that were already present during the 2019 tariff episode. Whereas the earlier episode remained largely consistent with a conventional safe-haven interpretation, the 2025 episode reflects the interaction of distinct shocks affecting confidence in U.S. institutions, Treasury-market intermediation, and the convenience value attached to dollar-denominated safe assets.

These findings complement the event-targeted VAR of Pinter et al. (2025). Their orthogonalised tariff-announcement shock explains much of the behaviour of equity prices, implied volatility, commodity prices, and short-term inflation expectations, while the persistent depreciation of the dollar and the behaviour of government bond yields are attributed to other orthogonal shocks. Our decomposition reaches a similar conclusion regarding the limits of a single tariff-announcement disturbance but goes one step further by identifying these additional disturbances as the *U.S. Institutional Credibility shock*, the *Treasury Market Intermediation shock*, and the *Safe-Asset Convenience shock*.

4 Conclusion

This paper studies the financial-market transmission of the April 2025 U.S. tariff announcements, with a particular focus on the unusual combination of dollar depreciation and rising long-term U.S. Treasury yields. Departing from event-based identification strategies that anchor the analysis on a single announcement shock, we adopt a statistical identification approach that exploits time variation in second moments and excess kurtosis to recover the contemporaneous transmission of shocks across financial markets. This framework is particularly well suited to the April 2025 episode, which was characterised by large, heterogeneous disturbances, pronounced volatility shifts, and rapidly changing market conditions.

Our results show that the April 2025 tariff episode cannot be understood as the propagation of a single tariff-announcement or safe-haven shock. Instead, the impulse responses and historical decomposition reveal that different components of the financial-market response were driven by distinct orthogonal macro-financial shocks. Conventional safe-haven forces explain the initial broad risk-off response, particularly the behaviour of equity markets. However, they cannot account for the subsequent combination of dollar depreciation and rising long-term Treasury yields, which departs both from standard flight-to-safety dynamics and from canonical tariff-transmission mechanisms.

Instead, the evidence points to distinct shocks associated with conventional safe-haven demand, the *U.S. Institutional Credibility shock*, and the *Treasury Market Intermediation shock*, which together account for the bulk of the financial-market response during the April 2025 episode. The historical decomposition shows that these shocks dominate different financial variables rather than propagating uniformly across markets. This distinction reconciles the apparently contradictory behaviour of equity prices, exchange rates, and fixed-income markets following the tariff announcement. A fourth disturbance, the *Safe-Asset Convenience shock*, contributes less to the 2025 episode itself but is central to separating Dollar Convenience from Treasury Convenience as distinct dimensions of U.S. international privilege, rather than a single underlying safe-haven factor.

A key implication of these findings is that exchange-rate dynamics following major trade-policy announcements need not reflect the propagation of a single underlying economic force. Even when the initial announcement triggers a conventional risk-off response, subsequent price adjustments may be dominated by orthogonal macro-financial disturbances. More broadly, our results suggest that U.S. international privilege is best understood as comprising several distinct dimensions. Confidence in U.S. institutions, Treasury-market functioning, and the convenience value attached to dollar-denominated safe assets can evolve independently, making it essential to distinguish these mechanisms when interpreting periods of stress in the international monetary system.

References

Adrian, T., R. K. Crump, and E. Moench (2013). Pricing the term structure with linear regressions. *Journal of Monetary Economics 60*(3), 433–453.

Adrian, T., M. Fleming, and K. Nikolaou (2025). Us treasury market functioning from the global financial crisis to the pandemic. *Annual Review of Financial Economics 17*, 49–76.

Alessandria, G. A., J. Ding, S. Y. Khan, and C. B. Mix (2025). The tariff tax cut: Tariffs as revenue. Technical report, National Bureau of Economic Research.

Arias, J. E., J. F. Rubio-Ramírez, M. Shin, and D. F. Waggoner (2026). Inference based on time-varying svars identified with sign restrictions. *Review of Economic Studies*, rdag008.

Auclert, A., M. Rognlie, and L. Straub (2025). The macroeconomics of tariff shocks. Technical report, National Bureau of Economic Research.

Baumeister, C. and J. D. Hamilton (2019). Structural interpretation of vector autoregressions with incomplete identification: Revisiting the role of oil supply and demand shocks. *American Economic Review 109*(5), 1873–1910.

Bauwens, L. and M. Lubrano (1998). Bayesian inference on garch models using the gibbs sampler. *The Econometrics Journal 1*(1), C23–C46.

Bertsche, D. and R. Braun (2022). Identification of structural vector autoregressions by stochastic volatility. *Journal of Business & Economic Statistics 40*(1), 328–341.

Bianchi, J., S. Bigio, and C. Engel (2025). Scrambling for dollars: International liquidity, banks and exchange rates. Technical report, NBER Working Paper No. 29457, Revise and Resubmit, Review of Economic Studies.

Bianchi, J. and L. Coulibaly (2025). The optimal monetary policy response to tariffs. Technical report, NBER Working Paper No. 33560.

Boyarchenko, N., P. Gupta, N. Steele, and J. Yen (2018). Negative swap spreads. *Economic Policy Review 24*(2), 1–14.

Brunnermeier, M., D. Palia, K. A. Sastry, and C. A. Sims (2021). Feedbacks: financial markets and economic activity. *American Economic Review 111*(6), 1845–1879.

Bruno, V. and H. S. Shin (2017). Global dollar credit and carry trades: a firm-level analysis. *The Review of Financial Studies 30*(3), 703–749.

Cardani, R., M. Kühl, J. Peppel-Srebrny, and R. Strauch (2025). Exchange rate uncertainty, tariff hikes, and adjustment costs. VoxEU.org.

Cetorelli, N. and L. S. Goldberg (2012). Banking globalization and monetary transmission. *The Journal of Finance 67*(5), 1811–1843.

Chan, J. C. (2020). Large bayesian vars: A flexible kronecker error covariance structure. *Journal of Business & Economic Statistics 38*(1), 68–79.

Chan, J. C. and C. Y. Hsiao (2014). Estimation of stochastic volatility models with heavy tails and serial dependence. *Bayesian inference in the social sciences*, 155–176.

Chan, J. C., G. Koop, and X. Yu (2024). Large order-invariant bayesian vars with stochastic volatility. *Journal of Business & Economic Statistics 42*(2), 825–837.

Chan, J. C. C. (2024). Bvars and stochastic volatility. In M. P. Clements and A. B. Galvão (Eds.), *Handbook of Research Methods and Applications in Macroeconomic Forecasting*, Chapter 3, pp. 43–67. Cheltenham, UK: Edward Elgar Publishing.

Corsetti, G., S. Lloyd, E. Marin, and D. Ostry (2026). U.s. risk and treasury convenience. *Working Paper*.

Del Negro, M. and G. E. Primiceri (2015). Time varying structural vector autoregressions and monetary policy: a corrigendum. *The review of economic studies 82*(4), 1342–1345.

Du, W., J. Im, and J. Schreger (2018). The us treasury premium. *Journal of International Economics 112*, 167–181.

Du, W., R. Keerati, and J. Schreger (2026). Decoupling dollar and treasury privilege. *IMF Economic Review*.

Du, W., A. Tepper, and A. Verdelhan (2018). Deviations from covered interest rate parity. *The Journal of Finance 73*(3), 915–957.

Frankovic, I. and S. Karau (2026). Political pressure on the fed - is this time different? *Working Paper*.

Furceri, D., S. A. Hannan, J. D. Ostry, and A. K. Rose (2018). Macroeconomic consequences of tariffs. Technical report, National Bureau of Economic Research.

Georgiadis, G., G. J. Müller, and B. Schumann (2024). Global risk and the dollar. *Journal of Monetary Economics 144*, 103549.

Geweke, J. and G. Amisano (2010). Comparing and evaluating Bayesian predictive distributions of asset returns. *International Journal of Forecasting 26*(2), 216–230.

Gopinath, G., E. Boz, C. Casas, F. J. Díez, P.-O. Gourinchas, and M. Plagborg-Møller (2020). Dominant currency paradigm. *American Economic Review 110*(3), 677–719.

Gopinath, G. and J. C. Stein (2021). Banking, trade, and the making of a dominant currency. *The Quarterly Journal of Economics 136*(2), 783–830.

Gourinchas, P.-O. and H. Rey (2007). From world banker to world venture capitalist: Us external adjustment and the exorbitant privilege. In *G7 current account imbalances: sustainability and adjustment*, pp. 11–66. University of Chicago Press.

Gourinchas, P.-O. and H. Rey (2022, January). Exorbitant privilege and exorbitant duty. CEPR Discussion Paper DP16944, Centre for Economic Policy Research.

Habib, M. M. and L. Stracca (2012). Getting beyond carry trade: What makes a safe haven currency? *Journal of International Economics 87*(1), 50–64.

Hartley, J. and A. Rebucci (2025). Tariffs, the dollar, and equities: High-frequency evidence from the liberation day announcement. *VoxEU.org*.

Hartwig, B. (2024). Bayesian vars and prior calibration in times of covid-19. *Studies in Nonlinear Dynamics & Econometrics 28*(1), 1–24.

Hossfeld, O. and R. MacDonald (2015). Carry funding and safe haven currencies: A threshold regression approach. *Journal of International Money and Finance 59*, 185–202.

Ignatenko, A., A. Lashkaripour, L. Macedoni, and I. Simonovska (2025). Making america great again? the economic impacts of liberation day tariffs. *Journal of International Economics 157*, 104138.

Ivashina, V., D. S. Scharfstein, and J. C. Stein (2015). Dollar funding and the lending behavior of global banks. *The Quarterly Journal of Economics 130*(3), 1241–1281.

Jarocinski, M. (2024). Estimating the fed's unconventional policy shocks. *Journal of Monetary Economics 144*, 103548.

Jeanne, O. and J. Son (2024). To what extent are tariffs offset by exchange rates? *Journal of International Money and Finance 142*, 103015.

Jiang, Z., A. Krishnamurthy, and H. Lustig (2018). Foreign safe asset demand for us treasurys and the dollar. *AEA Papers and Proceedings 108*, 537–541.

Jiang, Z., A. Krishnamurthy, and H. Lustig (2021). Foreign safe asset demand and the dollar exchange rate. *The Journal of Finance 76*(3), 1049–1089.

Jiang, Z., A. Krishnamurthy, and H. Lustig (2024). Dollar safety and the global financial cycle. *Review of economic studies 91*(5), 2878–2915.

Jiang, Z., R. J. Richmond, and T. Zhang (2024). A portfolio approach to global imbalances. *The Journal of Finance 79*(3), 2025–2076.

Kalemli-Özcan, Ş., C. Soylu, and M. A. Yildirim (2025). Global networks, monetary policy and trade. Technical Report 33686, National Bureau of Economic Research.

Känzig, D. R. (2021). The macroeconomic effects of oil supply news: Evidence from opec announcements. *American Economic Review 111*(4), 1092–1125.

Kashyap, A. K., J. C. Stein, J. L. Wallen, and J. Younger (2025). Treasury market dysfunction and the role of the central bank. *Brookings Papers on Economic Activity 1*.

Kim, S., N. Shephard, and S. Chib (1998). Stochastic volatility: likelihood inference and comparison with arch models. *The review of economic studies 65*(3), 361–393.

Kociecki, A., C. Matthes, and M. Piffer (2025). A non-gaussian gdp anatomy. *Working Paper*.

Krishnamurthy, A. and H. N. Lustig (2019). Mind the gap in sovereign debt markets: The U.S. treasury basis and the dollar risk factor. In *Challenges for Monetary Policy*, pp. 445–507. Federal Reserve Bank of Kansas City.

Lanne, M., M. Meitz, and P. Saikkonen (2017). Identification and estimation of non-gaussian structural vector autoregressions. *Journal of Econometrics 196*(2), 288–304.

Li, D., L. Petrasek, and M. Tian (2026). Risk-averse dealers in a risk-free market—the role of trading desk risk limits. *Journal of Financial Economics 181*(C).

Maggiori, M., B. Neiman, and J. Schreger (2020). International currencies and capital allocation. *Journal of Political Economy 128*(6), 2019–2066.

Müller, G., G. Georgiadis, and B. Schumann (2023). Dollar trinity and the global financial cycle. Technical report, CEPR Discussion Papers.

Ostry, D., S. Lloyd, and G. Corsetti (2025). Trading blows: The exchange-rate response to tariffs and retaliations. Staff Working Paper 1139, Bank of England, London.

Payne, J. and B. Szoke (2025). The fragility of government funding advantage. *Princeton University Department of Economics*.

Pinter, G., F. Smets, and S. Üslü (2025). Market whiplash after the 2025 tariff shock: an event-targeted var approach. BIS Working Papers 1282, Bank for International Settlements.

Poworoznek, E., N. Anceschi, F. Ferrari, and D. Dunson (2021). Efficiently resolving rotational ambiguity in bayesian matrix sampling with matching. *arXiv preprint arXiv:2107.13783*.

Rey, H. (2015). Dilemma not trilemma: the global financial cycle and monetary policy independence. Technical report, National Bureau of Economic Research.

Rigobon, R. (2003). Identification through heteroskedasticity. *Review of Economics and Statistics 85*(4), 777–792.

Ritter, C. and M. A. Tanner (1992). Facilitating the gibbs sampler: the gibbs stopper and the griddy-gibbs sampler. *Journal of the American Statistical Association 87*(419), 861–868.

Rodríguez-Clare, A., M. Ulate, and J. P. Vasquez (2025). The 2025 trade war: Dynamic impacts across us states and the global economy. Technical report, National Bureau of Economic Research.

Shin, H. S. (2012). Global banking glut and loan risk premium. *IMF Economic Review 60*(2), 155–192.

Sims, C. A. (2021). Svar identification through heteroskedasticity with misspecified regimes. Discussion paper, Princeton University.

Villani, M. (2009). Steady-state priors for vector autoregressions. *Journal of Applied Econometrics 24*(4), 630–650.

Waggoner, D. F. and T. Zha (1999). Conditional forecasts in dynamic multivariate models. *Review of Economics and Statistics 81*(4), 639–651.

Waggoner, D. F. and T. Zha (2003). A gibbs sampler for structural vector autoregressions. *Journal of Economic Dynamics and Control 28*(2), 349–366.

Appendices

A Model details

The model is given as follows:

$$y_t = b_0 + B_1 y_{t-1} + \ldots + B_p y_{t-p} + A^{-1}\epsilon_t \tag{A.1}$$
$$\epsilon_t|\omega_t \sim \mathcal{N}(0, \Omega_t), \quad \Omega_t = diag(\omega_{1,t}e^{h_{1,t}}, \ldots, \omega_{N,t}e^{h_{N,t}}) \tag{A.2}$$
$$\omega_{i,t} \sim \mathcal{IG}\left(\frac{\nu_i}{2}, \frac{\nu_i}{2}\right), \quad \nu_i > 0 \tag{A.3}$$
$$h_{i,t} = \rho_i h_{i,t-1} + v_{i,t}, \quad |\rho_i| < 1, \quad v_{i,t} \sim \mathcal{N}(0, \sigma_i^2) \tag{A.4}$$
$$h_{i,1} \sim \mathcal{N}\left(0, \frac{\sigma_i^2}{1-\rho_i^2}\right) \tag{A.5}$$

where y_t is an $N \times 1$ vector of endogenous variables and ϵ_t contains structural shocks that are independent across equations and, conditional on their latent volatility states, independent across time. The structural matrix A is assumed to be invertible but otherwise unrestricted.

A.1 Likelihood function

The likelihood is easy to derive as the data are conditionally Gaussian. First, denote the collection of model parameters as Θ, including the log-volatility processes and latent scaling factors $\omega_{i,t}$. Next, write a generic observation at time t as:

$$y_t = B'x_t + A^{-1}\epsilon_t \tag{A.6}$$
$$x_t = [y'_{t-1}, \ldots, y'_{t-p}, 1]' \tag{A.7}$$

Stacking the transposed model equations below each other into the $T \times N$ matrix Y yields:

$$Y = XB + E(A^{-1})' \tag{A.8}$$

where the matrix X has the vectors x'_t as its rows. We then have the vectorized model as:

$$\text{vec}(Y) \equiv y = \tilde{X}\beta + (A^{-1} \otimes I_T)\epsilon \tag{A.9}$$
$$\tilde{X} \equiv (I_N \otimes X) \tag{A.10}$$
$$\epsilon \sim \mathcal{N}(0, \Omega) \tag{A.11}$$
$$\Omega = \text{diag}(\omega_{1,1}e^{h_{1,1}}, \ldots, \omega_{1,T}e^{h_{1,T}}, \ldots, \omega_{N,1}e^{h_{N,1}}, \ldots, \omega_{N,T}e^{h_{N,T}}) \tag{A.12}$$

It then follows that the likelihood function is given by:

$$p(y|\theta) \propto |\det(A)|^T \det(\Omega)^{-1/2} e^{-\frac{1}{2}(y-\tilde{X}\beta)'\tilde{\Omega}^{-1}(y-\tilde{X}\beta)} \tag{A.13}$$

where $\tilde{\Omega} = (A^{-1} \otimes I_T)\Omega(A^{-1} \otimes I_T)'$.

A.2 Prior distributions

The prior on the impact matrix is an improper flat prior, $p(\alpha) \propto 1$. In our conjugate MCMC derivations, this is implemented computationally by setting the prior precision matrix $K_\alpha = 0$ and the prior mean vector $\alpha_0 = 0$, so that the prior contribution vanishes from the conditional posterior precision. One could set an informative prior here as in Brunnermeier et al. (2021) which would also help mitigate the rotational ambiguity present in this model, but we refrain from doing so because there is no clear guidance as to how to specify the elements of this matrix, and we wish to impose as little identifying assumptions on the model as possible.

Next, we assume a Normal distribution for the VAR parameters:

$$\beta \sim \mathcal{N}(\beta_0, V_\beta) \tag{A.14}$$

which is parameterized in the conventional Minnesota fashion. The elements of β_0 are set equal to zero, except for the first autoregressive coefficients in each equation that are set to one for variables in log-levels and zero for variables expressed as interest rates and spreads. The elements of V_β are set as follows. For coefficients belonging to the lags of the variable in equation i we set the prior variance equal to $\left(\lambda_1 k^{-\lambda_3}\right)^2$. For coefficients belonging to another variable j we set the prior variance equal to $\left(\lambda_1 \lambda_2 k^{-\lambda_3} \frac{s_i}{s_j}\right)^2$. The terms s_i^2 are obtained as residual variances from univariate AR(p) models. The overall shrinkage parameter λ_1 is set to 0.2, the cross-variable shrinkage parameter λ_2 is set to 0.5, and the lag-decay parameter λ_3 equals 1. Lastly, for the constant term in equation i we set the prior variance equal to $100 s_i^2$.

The prior on the degrees of freedom controls the prior degree of non-Gaussianity and we use a truncated Gamma distribution:

$$\nu_i \sim \mathcal{G}(s_\nu, \delta_\nu) \mathbb{1}_{\nu_i \in [\underline{\nu}, \overline{\nu}]} \tag{A.15}$$

We tilt the odds towards the Gaussian model by setting $s_\nu = 4$ and $\delta_\nu = 5$, implying a mean of 20 and variance 100 before truncation. The lower bound is set to $\underline{\nu} = 0.1$ to avoid the singularity problems occurring for very small degrees of freedom outlined in Bauwens and Lubrano (1998), while the upper bound $\overline{\nu} = 50$ ensures that we do not assign too much prior weight to the Gaussian model.

Lastly, regarding the stochastic volatility parameters of the model we set the following prior distributions:

$$\rho_i \sim \mathcal{N}(\rho_0, V_\rho) \mathbb{1}_{|\rho_i|<1} \tag{A.16}$$

$$\sigma_i^2 \sim \mathcal{IG}\left(\frac{s_\sigma}{2}, \frac{\delta_\sigma}{2}\right) \tag{A.17}$$

where the hyperparameters are set to $\rho_0 = 0.95$, $V_\rho = 0.05^2$, $s_\sigma = 6$, and $\delta_\sigma = 0.2$.

A.3 MCMC algorithm

To help with the exposition of the MCMC algorithm we first write out the necessary terms of the posterior density to be sampled from. For this, multiply the likelihood function

with the prior, assuming prior independence across the parameter blocks, which yields:

$$
\begin{aligned}
p(\Theta|y) \propto & \underbrace{|\det(A)|^T \det(\Omega)^{-1/2} e^{-\frac{1}{2}(y-\tilde{X}\beta)'\tilde{\Omega}^{-1}(y-\tilde{X}\beta)}}_{p(y|\Theta)} \\
& \cdot \underbrace{e^{-\frac{1}{2}(\beta-\beta_0)'V_\beta^{-1}(\beta-\beta_0)}}_{p(\beta)} \\
& \cdot \underbrace{\prod_i \left(\frac{\sigma_i^2}{1-\rho_i^2}\right)^{-1/2} e^{-\frac{(1-\rho_i^2)h_{i,1}^2}{2\sigma_i^2}} (\sigma_i^2)^{-\frac{T-1}{2}} e^{-\frac{1}{2\sigma_i^2}\sum_{t=2}^T (h_{i,t}-\rho_i h_{i,t-1})^2}}_{p(h|\rho,\sigma^2)} \\
& \cdot \underbrace{\prod_i e^{-\frac{1}{2}(\rho_i-\rho_0)'V_\rho^{-1}(\rho_i-\rho_0)} \mathbb{1}_{\rho_i\in(-1,1)} \cdot (\sigma_i^2)^{-\left(\frac{s_\sigma}{2}+1\right)} e^{-\frac{\delta_\sigma}{2\sigma_i^2}}}_{p(\rho,\sigma^2)} \\
& \cdot \underbrace{\prod_i \Gamma\left(\frac{\nu_i}{2}\right)^{-T} \left(\frac{\nu_i}{2}\right)^{T\nu_i/2} \prod_t \omega_{i,t}^{-\left(\frac{\nu_i}{2}+1\right)} e^{-\frac{\nu_i}{2\omega_{i,t}}}}_{p(\omega|\nu)} \\
& \cdot \underbrace{\prod_i \nu_i^{s_\nu-1} e^{-\frac{\nu_i}{\delta_\nu}} \mathbb{1}_{\nu_i\in[\underline{\nu},\overline{\nu}]}}_{p(\nu)}
\end{aligned}
\tag{A.18}
$$

Recall that we set a flat prior on A so that its prior density does not show up. An informative prior can be added, as long as it is Gaussian and the rows of A are a priori independent. The above density is not tractable and MCMC methods are used to draw samples from it. In the following we write all distributions conditional on the data y and the parameter vector θ, where, to avoid notational clutter, it is understood that the respective parameter to be sampled is not part of the conditioning set.

Step 1. Draw from $p(\alpha|y,\theta) = p(\alpha|y,\beta,\omega,\nu,h)$.
To sample from this density we follow directly the algorithm outlined in Chan et al. (2024) to sample each row of A conditional on the other rows, which is an application of results in Waggoner and Zha (2003) and Villani (2009). To this end, write the model for row i as:

$$(Y - XB)a_i = E_i \tag{A.19}$$
$$E_i \sim \mathcal{N}(0, \Omega_i) \tag{A.20}$$
$$\Omega_i = \text{diag}(\omega_{i,1}e^{h_{i,1}}, \ldots, \omega_{i,T}e^{h_{i,T}}) \tag{A.21}$$

The authors then show that one can produce a draw for α_i by drawing the elements of this vector from:

$$\alpha_i(1) \sim \mathcal{AN}\left(\phi_1, T^{-1}\right) \tag{A.22}$$
$$\alpha_i(j) \sim \mathcal{N}\left(\phi_j, T^{-1}\right), \quad j = 2, \ldots, N \tag{A.23}$$

where, for each element $j = 1, \ldots, N$, the means of these distributions are given by:

$$\phi_j = \hat{a}_i' C_i v_j \tag{A.24}$$
$$\hat{a}_i = \bar{K}_{\alpha_i}^{-1} K_{\alpha_i} \alpha_{0,i} \tag{A.25}$$
$$\bar{K}_\alpha = K_{\alpha_i} + (Y - XB)' \Omega_i^{-1} (Y - XB) \tag{A.26}$$
$$C_i C_i' = T^{-1} \bar{K}_{\alpha_i} \tag{A.27}$$
$$v = (v_1, v_2, \ldots, v_N) \tag{A.28}$$
$$v_1 = C_i^{-1} (A_{-i}')^\perp / ||C_i^{-1} (A_{-i}')^\perp|| \tag{A.29}$$
$$(v_2, \ldots, v_N) = v_1^\perp \tag{A.30}$$

and $x^\perp$ denotes the orthogonal complement of x, while A_{-i} is the matrix A with its i-th row deleted. Note that (A.27) is meant as a computational instruction that states to compute C_i as the lower triangular Cholesky factorization of $T^{-1}\bar{K}_{\alpha_i}$. How to draw from the absolute normal distribution is outlined in Villani (2009).

Step 2. Draw from $p(\beta|y, \theta) = p(\beta|y, \alpha, \omega, h)$.
From standard arguments then follows the usual Gaussian conditional posterior for β:

$$\beta|y, \theta \sim \mathcal{N}(\bar{\beta}, \bar{V}_\beta) \tag{A.31}$$
$$\bar{V}_\beta = \left(V_\beta^{-1} + (A \otimes X)' \Omega^{-1} (A \otimes X)\right)^{-1} \tag{A.32}$$
$$\bar{\beta} = \bar{V}_\beta \left(V_\beta^{-1} \beta_0 + (A \otimes X)' \Omega^{-1} \operatorname{vec}(Y A')\right) \tag{A.33}$$

In practice, we do not compute the inverse matrix, but rather work with the precision matrix, which makes for more efficient sampling (see Chan (2020) for implementation details).

Step 3. Draw from $p(\omega|y, \theta) = \prod_t \prod_i p(\omega_{i,t}|y, \alpha, \beta, h_i, \nu_i)$.
We first purge the structural shocks of the stochastic volatility parameters via $E = ((Y - XB)A') \odot O^{-1/2}$, where the entries of the $T \times N$ matrix O are $e^{h_{i,t}}$, and $\odot$ denotes the Hadamard product (i.e. element-wise multiplication). Then, with these shocks in hand it is easy to verify that the conditional posterior distributions are given by:

$$\omega_{i,t}|y, \theta \sim \mathcal{IG}\left(\frac{\nu_i + 1}{2}, \frac{\nu_i + e_{i,t}^2}{2}\right) \tag{A.34}$$

Step 4. Draw from $p(\nu|y, \theta) = \prod_i p(\nu_i|\omega_i)$.
As for the previous step the degrees of freedom parameters occur in the expressions for the structural errors of equation i, the prior densities for $\omega_{i,t}$, and in their own priors. Hence we have:

$$p(\nu_i|y, \theta) \propto p(\nu_i) \Gamma\left(\frac{\nu_i}{2}\right)^{-T} \left(\frac{\nu_i}{2}\right)^{\frac{T\nu_i}{2}} \prod_t \omega_{i,t}^{-\frac{\nu_i}{2}} e^{-\frac{1}{\omega_{i,t}} \frac{\nu_i}{2}} \tag{A.35}$$

where $p(\nu_i)$ is the prior density given above. This density is again non-standard and again we draw from it using a Griddy-Gibbs sampling step.

Step 5. Draw from $p(\sigma^2|y,\theta) = \prod_i p(\sigma_i^2|h_i,\rho_i)$.
This step is standard, as the conditional posterior takes the simple form:

$$\sigma_i^2|y,\theta \sim \mathcal{IG}\left(\frac{s_\sigma + T}{2}, \frac{\delta_\sigma + (1-\rho_i^2)h_{i,1}^2 + \sum_{t=2}^{T}(h_{i,t} - \rho_i h_{i,t-1})^2}{2}\right) \tag{A.36}$$

Step 6. Draw from $p(\rho|y,\theta) = \prod_i p(\rho_i|h_i,\sigma_i^2)$.
From the prior distribution and the log-volatility process it is easy to derive that the conditional posterior is proportional to the following density:

$$p(\rho_i|h_i,\sigma_i^2) \propto p(\rho_i)g(\rho_i)e^{-\frac{1}{2\sigma_i^2}\sum_{t=2}^{T}(h_{i,t}-\rho_i h_{i,t-1})^2} \tag{A.37}$$

$$g(\rho_i) = (1-\rho_i^2)^{1/2}e^{-\frac{1}{2\sigma_i^2}(1-\rho_i^2)h_{i,1}^2} \tag{A.38}$$

This density is non-standard and we draw from it using a Griddy-Gibbs step.

Step 7. Draw from $p(h|y,\theta) = \prod_i p(h_i|y,A,\beta,\rho_i,\sigma_i^2,\gamma_i,\nu_i,\omega_i)$.
We use the auxiliary mixture sampler from Kim et al. (1998) to sample from this density. As the data in this sampling step for equation i we use column i of $E = ((Y - XB)A') \odot O^{-1/2}$, where this time the entries of the matrix O are $\omega_{i,t}$. The implementation of the sampling step is well explained in Chan and Hsiao (2014), and we refer to both references for further details on the implementation. We only note that it is important to draw the mixture indicators before the log-volatilities in order to sample from the correct conditional posterior (see Del Negro and Primiceri (2015) and Chan (2024)).

A.4 Resolving rotational ambiguity

The rotational ambiguity in the model arises because one can always define a signed permutation matrix P_s such that the following reduced form error terms are observationally equivalent:

$$A^{-1}\epsilon_t = A^{-1}P_s P_s'\epsilon_t \equiv \tilde{A}^{-1}\tilde{\epsilon}_t \tag{A.39}$$

Note that the rotation matrices in models such as ours are restricted to signed column permutations. In contrast, in the usual Gaussian VAR model any conceivable orthogonal matrix is allowed for, making the identification issue more prevalent there (see also the discussions in Lanne et al. (2017) and Bertsche and Braun (2022) and the references therein). While non-Gaussianity can provide additional identifying information through higher-order moments, identification in our framework primarily relies on variation in second moments. Resolving the permutation ambiguity merely requires mapping the posterior draws consistently to the neighborhood of one arbitrarily chosen posterior mode. Intuitively, imagine a simple supply-demand setup with two structural shocks that is statistically identified, and that we have two draws for the impact matrix:

$$A_1^{-1} = \begin{pmatrix} 0.8 & 0.5 \\ 1.2 & -0.8 \end{pmatrix}, \quad A_2^{-1} = \begin{pmatrix} 0.5 & -0.8 \\ -0.8 & -1.2 \end{pmatrix} \tag{A.40}$$

Clearly, both matrices contain the same information about the effects of the shocks; one need only reorder the columns and switch the sign of the second column in A_2^{-1} to perfectly recover A_1^{-1}. This illustrates that the permutation issue has no impact on identification. It needs to be resolved, however, because in summary statistics across a sample of raw posterior draws, the opposing signs and column switches will cancel out and mask the economic content of the shocks. To do so, we use the approaches from Poworoznek et al. (2021) and Kociecki et al. (2025). Namely, given a MCMC sequence of draws for the impact matrix $D_{(m)} \equiv A_{(m)}^{-1}$ for $m = 1, \dots, M$, we wish to find sign-permutations for each draw that minimize the squared Frobenius norm between the draws and some reference matrix $\hat{D} \equiv \hat{A}^{-1}$:

$$\min_{\{P_{s,(m)}\}} \sum_{m=1}^{M} ||D_{(m)}P_{s,(m)} - \hat{D}||_{\hat{A}}^2 = \min_{\{P_{s,(m)}\}} \sum_{m=1}^{M} \operatorname{tr}\left((D_{(m)}P_{s,(m)} - \hat{D})'\hat{A}'\hat{A}(D_{(m)}P_{s,(m)} - \hat{D})\right) \tag{A.41}$$

Clearly, this is a minimization problem for each draw individually. Let us denote by tr_m the trace term for draw m. Expanding out this term gives

$$\mathrm{tr}_m = \operatorname{tr}\left(P_{s,(m)}'D_{(m)}'\hat{A}'\hat{A}D_{(m)}P_{s,(m)}\right) - 2\operatorname{tr}\left(\hat{D}'\hat{A}'\hat{A}D_{(m)}P_{s,(m)}\right) + \operatorname{tr}\left(\hat{D}'\hat{A}'\hat{A}\hat{D}\right) \tag{A.42}$$

$$= \operatorname{tr}\left(D_{(m)}'\hat{A}'\hat{A}D_{(m)}\right) - 2\operatorname{tr}\left(\hat{A}D_{(m)}P_{s,(m)}\right) + N \tag{A.43}$$

Hence, we only need to consider the middle term of the last expression as the other terms are unaffected by the choice of signed permutation matrix. This is the approach proposed by Kociecki et al. (2025), and they show that one can equivalently solve the following modified problem:

$$\max_{P_{(m)}} \operatorname{tr}\left(|\hat{A}D_{(m)}|P_{(m)}\right) \tag{A.44}$$

where the absolute value is taken element-wise. Note here that thanks to the absolute value, the solution is simply a permutation matrix and the solution can be found easily using the built-in MATLAB function 'matchpairs'. For the algorithm we set the cost of an unmatched pair to zero with the maximization option of the function. We depart from Kociecki et al. (2025) in that we do not use the maximum likelihood estimator of A, but instead follow Poworoznek et al. (2021) and choose the sampled impact matrix with median condition number. Specifically, for the raw MCMC draws we first compute the condition number of each impact matrix. Second, we find the impact matrix with minimum Euclidean distance of its condition number to the median condition number, and take its inverse to obtain $\hat{A}$. After finding the optimal unsigned permutation $P_{(m)}$, we recover the required sign for each matched column by extracting the sign of the corresponding element directly from the original, un-absoluted matrix $\hat{A}D_{(m)}$, and apply these signs to construct the final signed permutation matrix $P_{s,(m)}$.

A.5 Implementation of the Griddy-Gibbs sampling step

In the above we draw some parameters using discrete approximations to the true conditional posteriors. Here we describe the general algorithm based on the exposition

in Ritter and Tanner (1992), assuming that the generic density in question, $p(x)$, is univariate and its support is bounded, i.e. $x \in [\underline{x}, \overline{x}]$ where the bounds are finite. The integrating constant of the density does not need to be known. The random draw generation then proceeds as follows. First, create an evenly spaced, ordered grid x_k of K points. In our application we use 500 grid points. Next, evaluate the log of the target density at each grid point, giving $l_k \equiv \log(p(x_k))$ and record the largest value $l^M = \max_k(l_k)$. Then, adjust the probabilities via $\tilde{l}_k = l_k - l^M$ and calculate the grid point probabilities p_k as:

$$p_k = e^{\tilde{l}_k - \log\left(\sum_k e^{\tilde{l}_k}\right)} \tag{A.45}$$

This "LogSumExp" trick is a numerically stable way to calculate the probabilities, and one can verify that $p_k \geq 0 \; \forall k$ and $\sum_k p_k = 1$. Next, cumulate these probabilities to obtain an approximate CDF, denoted F. To produce a draw from this distribution, draw a uniform number $u \in [F_1, F_K]$ and locate the grid points x_j and x_{j+1} such that $u \in [F_j, F_{j+1}]$. Lastly, use a linear approximation of the CDF between these grid points and invert this linear function to find the final draw as:

$$x^* = x_j + \frac{u - F_j}{F_{j+1} - F_j}(x_{j+1} - x_j) \tag{A.46}$$

A.6 Predictive log likelihood calculations

The predictive log likelihood implied by the one-step-ahead predictive density can be constructed recursively. As in Geweke and Amisano (2010), we start from the following decomposition, where M_j denotes model j and y^t are the data up to and including time t:

$$\log(p(y^T|M_j)) = \sum_{t=1}^{T} \log(p(y_t|y^{t-1}, M_j)) \tag{A.47}$$

Hence, to evaluate the predictive log likelihood one simply sums the individual one-step-ahead out-of-sample predictive density evaluations. However, the fact that the decomposition is based on out-of-sample predictive densities makes it impractical for all time periods of the sample. It is common practice to start the summation at some sufficiently large time point and instead calculate:

$$\log(p(y^T|y^{T_0}, M_j)) = \sum_{t=T_0+1}^{T} \log(p(y_t|y^{t-1}, M_j)) \tag{A.48}$$

If T_0 is sufficiently large the influence of the prior on the predictive densities is small and the data dominate in the model comparison. The remaining step is to evaluate the predictive density conditional on each recursive sample y^{t-1}, which can be written as

$$p\left(y_t|y^{t-1}, M_j\right) = \int_{\Theta_j} p\left(y_t|y^{t-1}, \Theta_j, M_j\right) p\left(\Theta_j|y^{t-1}, M_j\right) \mathrm{d}\Theta_j \tag{A.49}$$

$$\approx \frac{1}{S}\sum_{s=1}^{S} p\left(y_t|y^{t-1}, \Theta_j^{(s)}, M_j\right) \tag{A.50}$$

where S is a MCMC sample with which one can approximate the exact integral over the parameters Θ_j of model j.
It remains to show how we evaluate the predictive densities, for which we first define $\log\left(p\left(y_t|y^{t-1},\Theta_j^{(s)},M_j\right)\right) \equiv L(s,j)$ for the different models. First, we recap the model for convenience:

$$y_t = B'x_t + A^{-1}O_t^{1/2}v_t \tag{A.51}$$

$$\Rightarrow v_t = O_t^{-1/2}A(y_t - B'x_t) \tag{A.52}$$

$$O_t = diag(e^{h_{1,t}},\ldots,e^{h_{N,t}}) \tag{A.53}$$

where x_t contains the relevant data until time $t-1$ and $B'x_t$ denotes the conditional mean of y_t given the data and parameters. With parameter draws for A, B, h, and ν, as well as the out-of-sample observations y_t, one can compute all terms above. Values for $h_{i,t}$ can be generated from the individual autoregressive processes above.
When the model includes stochastic volatility but not heavy tails, v_t follows a multivariate standard normal distribution. The predictive density is therefore

$$L(s,j) = -\frac{N}{2}\log(2\pi) - \frac{1}{2}\log(\det(V_y)) - \frac{1}{2}(y_t - B'x_t)'V_y^{-1}(y_t - B'x_t) \tag{A.54}$$

$$V_y = A^{-1}O_t\left(A^{-1}\right)' \tag{A.55}$$

The determinant term in V_y incorporates the Jacobian of the transformation from the structural shocks to y_t.
When the model includes heavy-tailed shocks, the elements of v_t follow independent Student-t distributions with ν_i degrees of freedom. The absolute value of the determinant of the Jacobian of the inverse transformation from v_t to y_t is $|\det(O_t^{-1/2})||\det(A)| = \exp\left(-\frac{1}{2}\sum_{i=1}^N h_{i,t}\right)|\det(A)|$. Hence, the predictive density conditional on parameters in this case is:

$$\begin{aligned} L(s,j) = \log(|\det(A)|) - \frac{1}{2}\sum_{i=1}^N h_{i,t} \\ + \sum_{i=1}^N\left[\log(\Gamma((\nu_i+1)/2)) - \log(\Gamma(\nu_i/2)) - \frac{1}{2}\log(\pi\nu_i)\right] \\ - \sum_{i=1}^N \frac{\nu_i+1}{2}\log\left(1 + \frac{e^{-h_{i,t}}\epsilon_{i,t}^2}{\nu_i}\right) \end{aligned} \tag{A.56}$$

The structural errors are calculated from the model equations above. When stochastic volatility is not present in the model we have $h_{1,t} = \cdots = h_{N,t} = 0$.
Once we have calculated $L(s,j)$ for every s we need to take the average over the exponentials of these values. To do so in a numerically stable way we again use the

"LogSumExp" trick:

$$\log\left(p\left(y_t|y^{t-1}, M_j\right)\right) \approx \log\left(\frac{1}{S}\sum_{s=1}^{S} p\left(y_t|y^{t-1}, \Theta_j^{(s)}, M_j\right)\right) \tag{A.57}$$

$$= \log\left(\frac{1}{S}\sum_{s=1}^{S} \exp\left(L(s,j)\right)\right) \tag{A.58}$$

$$= \log\left(\frac{1}{S}\sum_{s=1}^{S} \exp\left(L(s,j) - L^*\right)\right) + L^* \tag{A.59}$$

$$L^* = \max_s\{L(s,j)\} \tag{A.60}$$

When stochastic volatility is present, to improve the accuracy of the computations, for each s we simulate 100 values for $h_{i,t}$ and expand the average across these additional draws.

B Application to Oil Price Data

This section follows the empirical set-up of Bertsche and Braun (2022) and applies our model to the same four-variable oil market VAR. The dataset consists of monthly observations for 1974:01–2016:12 and is specified as

$$y_t = \left[100\Delta q_t,\ 100\Delta wip_t,\ 100p_t,\ 100\Delta inv_t\right]',$$

where q_t, wip_t, and p_t denote the natural logarithms of global crude oil production (in million barrels per day), world industrial production (following Baumeister and Hamilton (2019)), and the real WTI oil price, respectively, while Δinv_t captures the change in global oil inventories, expressed as a fraction of the previous period's oil production and left in levels rather than logs since it can be negative. Consequently, $100\Delta q_t$ and $100\Delta wip_t$ enter as approximate percentage growth rates, $100p_t$ enters in scaled log-levels, and $100\Delta inv_t$ enters as a percentage of lagged production. We use twelve lags, consistent with the literature, and exclude pre-1974 observations when U.S. oil prices were regulated.

The analysis compares the results of Bertsche and Braun (2022) with three variants of the model proposed in this paper:

1. a t-Distribution specification,
2. an SV specification, and
3. an SV-t specification.

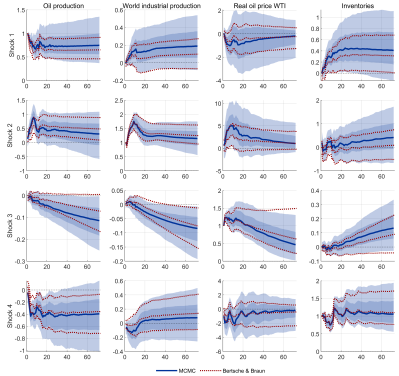
Figure B.1 presents impulse responses for the conventional oil supply shock under all three variants. Because the three specifications share the same data, variable ordering, and lag structure, we report the shock occupying the same position across all three variants; as the sign of any individual shock is a normalization choice without economic content (Appendix A.4), we additionally fix each shock's sign relative to the frequentist

benchmark of Bertsche and Braun (2022) for visual comparability. The t-Distribution model aligns closely with the frequentist stochastic-volatility benchmark of Bertsche and Braun (2022), confirming that modelling fat-tailed structural shocks provides a parsimonious way of accommodating extreme observations and delivers impulse responses that are empirically similar to those obtained under heteroskedastic identification.

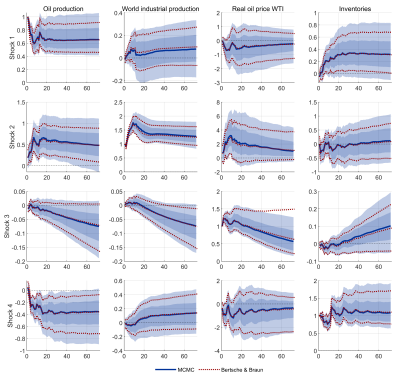
Across all variables, the SV, t-Distribution, and SV-t models produce very similar impulse responses. Consistent with Bertsche and Braun (2022), structural inference is robust when the data contain sufficiently informative variation in second moments, excess kurtosis, or both. The t-Distribution model is particularly noteworthy: despite its parsimony—adding only a single degrees-of-freedom parameter per equation—it reproduces essentially the same dynamic responses as the richer SV specification. The conventional oil supply shock (shock 1) produces a rise in production, an increase in world industrial activity, and a decline in real oil prices, in line with Känzig (2021) and the benchmark responses in Bertsche and Braun (2022). The oil price news shock (shock 3) raises real oil prices without an immediate decline in production and induces inventory adjustment over the medium term, again closely matching the patterns in Bertsche and Braun (2022). The fact that these qualitative and quantitative features are reproduced under all three specifications indicates that the empirical conclusions are robust across alternative specifications of the structural-shock distribution, even when using the more parsimonious t-Distribution model.

Figure B.2 compares the estimated log-volatilities under our Bayesian specifications with those obtained by Bertsche and Braun (2022). The volatility paths are remarkably similar across approaches, with pronounced spikes coinciding with well-known geopolitical and energy-market events. This reinforces the conclusion that the substantive economic interpretation is robust to alternative specifications of the structural-shock distribution. Volatility in oil production rises sharply during the oil crises of the 1970s and again around the Gulf War and the 2008 financial crisis. World industrial production volatility mirrors global business-cycle fluctuations, with frequent swings in the 1970s-1980s, relative stability during the 1990s aside from the Asian crisis, and a marked surge in 2008-09. Oil price volatility is highly sensitive to energy-market disruptions and geopolitical tensions, exhibiting extreme values in the 1970s, elevated levels in the 1980s, and strong increases in the 2000s. Inventory volatility remains comparatively subdued, consistent with its role in buffering short-run demand-supply imbalances.

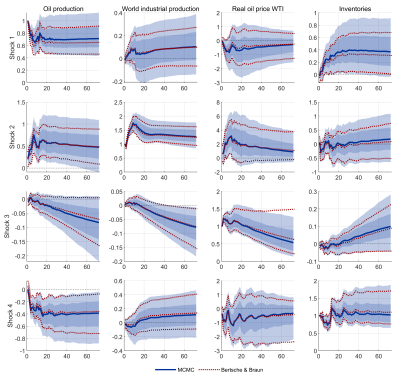
Figure B.3 shows that the posterior degrees of freedom vary markedly across equations. In the t-Distribution specification, low degrees of freedom are most evident for oil production, world industrial production, and inventories, while the real oil price equation is associated with substantially higher values. Once stochastic volatility is introduced in the SV-t specification, the evidence for heavy tails becomes more selective, remaining most pronounced for world industrial production and weakening for the other equations. This pattern suggests that part of the apparent non-Gaussianity in the shocks reflects time-varying volatility, so that the role of the Student-t component is heterogeneous across variables and partly subsumed by stochastic volatility.



(a) t-Distribution



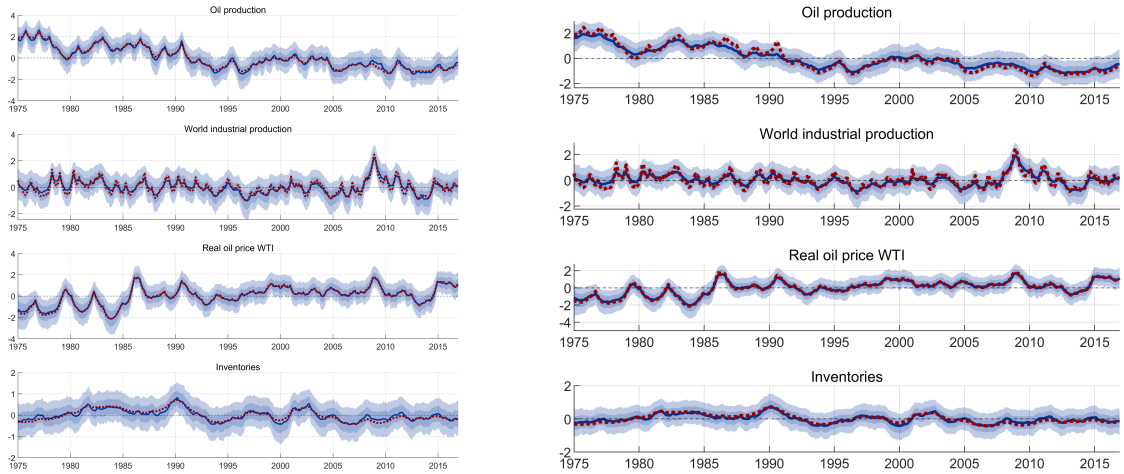
(b) SV



(c) SV-t

Figure B.1: Impulse responses in the oil-market application.

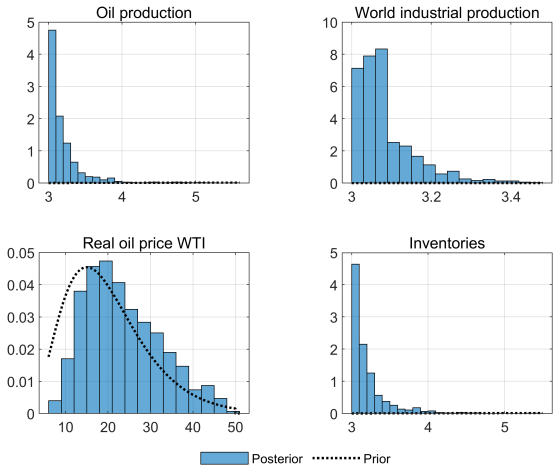
Notes: Impulse responses to the statistically identified structural shocks in the oil-market application over a horizon of 72 months. Panels (a)–(c) report results from the t-Distribution, stochastic volatility (SV), and combined SV-t specifications, respectively. Solid blue lines denote posterior median impulse responses, while the shaded areas represent 68% and 95% posterior credible intervals. Red dotted lines report the corresponding responses from Bertsche and Braun (2022).



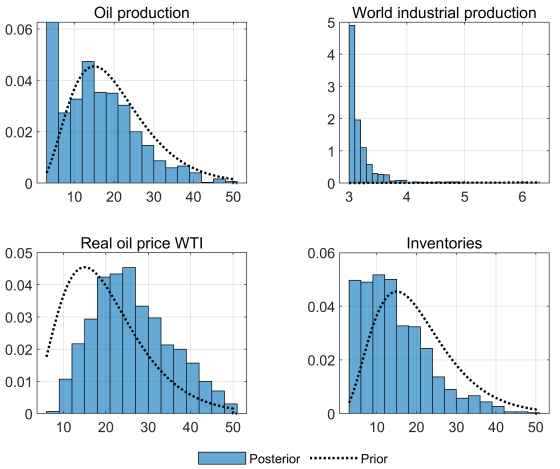
(a) SV (b) SV-t

Figure B.2: Estimates of log volatilities.

Notes: The figure reports Bayesian estimates of the log-volatility process $h_{i,t}$ for each variable. The dark blue line denotes the posterior median, while the darker and lighter shaded areas represent the 68% and 95% posterior credible intervals, respectively. The red dotted line reports the corresponding frequentist estimate from Bertsche and Braun (2022).



(a) t-Distribution



(b) SV-t

Figure B.3: Posterior degrees of freedom.

Notes: Histograms of posterior draws of the degrees of freedom of each structural shock. The dashed line corresponds to the prior distribution evaluated at grid points covering the posterior draws.

C Additional Results: Financial Market Dynamics Around the 2025 Tariff Announcement

This section reports additional results supporting the empirical analysis of financial-market dynamics around the April 2025 tariff announcement. Table C.1 summarizes the ten endogenous variables in the baseline model.

Table C.1: Data description, transformations, and sources

	Series	Definition	Transf.	Key	Source
1	S&P 500	Broad U.S. equity price index	log ×100	SPX	Refinitiv
2	VIX	Chicago Board Options Exchange implied volatility index (percent)	level	VIXCLS	FRED
3	EUR per USD exchange rate	Euros per U.S. dollar; constructed as the inverse of the euro–dollar rate (dollars per euro)	log ×100	EUR=	Refinitiv
4	π_{1Y}^{swap}	One-year U.S. inflation-linked swap rate (percent)	level	USCPIZ1Y=	Refinitiv
5	Treasury term premium (3M)	Three-month U.S. Treasury term premium from the Adrian–Crump–Moench (ACM) model (percent)	level	—	Adrian et al. (2013)
6	US 10Y yield	Ten-year U.S. Treasury benchmark yield (percent)	level	US10YT=RR	Refinitiv
7	EA 10Y yield	Ten-year euro-area benchmark government bond yield, proxied by the German Bund (percent)	level	DE10YT=RR	Refinitiv
8	Swap spread (10Y)	Ten-year USD interest rate swap rate minus ten-year U.S. Treasury yield (percentage points)	level	—	Constructed
9	Dollar convenience (10Y)	Ten-year G10 benchmark CIP deviation; daily cross-currency median, 13-day moving average (basis points)	level	—	Du et al. (2026, 2018)
10	Treasury convenience (10Y)	G10 median ten-year government-bond CIP deviation; 13-day moving average (basis points)	level	—	Du et al. (2018, 2026)

Notes: The estimation sample runs from 2 January 2008 to 15 May 2025 at daily frequency; the sample start is dictated by the availability of Dollar Convenience (10Y), the latest-starting endogenous series. The table reports the ten endogenous variables of the baseline VAR specification. The EUR per USD exchange rate is constructed as the inverse of the euro–dollar rate so that the series rises with dollar appreciation. The three-month Treasury term premium follows the ACM estimation procedure in Adrian et al. (2013). The Swap spread (10Y) is computed as the difference between the ten-year USD swap rate and the ten-year U.S. Treasury yield. *Transf.* denotes the transformation applied prior to estimation: equity and exchange-rate series enter in log levels multiplied by 100, while yields, spreads, term-premium estimates, and CIP deviations enter in levels (percent or basis points as indicated). FRED refers to the Federal Reserve Economic Data database.

Swap–Treasury Spread (10Y). The ten-year Swap–Treasury spread is defined as the fixed rate on a ten-year U.S. dollar interest rate swap minus the ten-year U.S. Treasury benchmark yield:

$$\text{Swap–Treasury spread}_{n,t} = y_{n,t}^{\text{swap}} - y_{n,t}^{\text{UST}}.$$

The spread compares two ways of obtaining duration exposure—through swaps or by holding cash Treasuries. A higher spread indicates that Treasuries are expensive relative to swaps; a more negative spread indicates that Treasuries are cheap relative to swaps, which is commonly associated with limits to arbitrage, dealer balance-sheet constraints, and impaired Treasury-market intermediation (Boyarchenko et al., 2018; Kashyap et al., 2025). After the Global Financial Crisis, swap spreads in the U.S. turned persistently negative, a pattern that deepened further around the March 2020 Treasury-market turmoil and again in 2025 (Du et al., 2026).

Dollar Convenience (10Y). Dollar Convenience is the benchmark covered interest parity (CIP) deviation as defined in Du, Tepper, and Verdelhan (2018) and Du et al. (2026). It compares the return on a synthetic dollar risk-free asset—obtained by investing in a foreign risk-free instrument and hedging the exchange-rate risk through an FX swap—with the return on a cash-market dollar risk-free asset at the same maturity:

$$x_{i,n,t}^{Rf} = \underbrace{\left(y_{i,n,t}^{Rf} - \rho_{i,n,t}\right)}_{\text{FX-swap-implied dollar rate}} - \underbrace{y_{\$,n,t}^{Rf}}_{\text{cash-market dollar rate}}$$

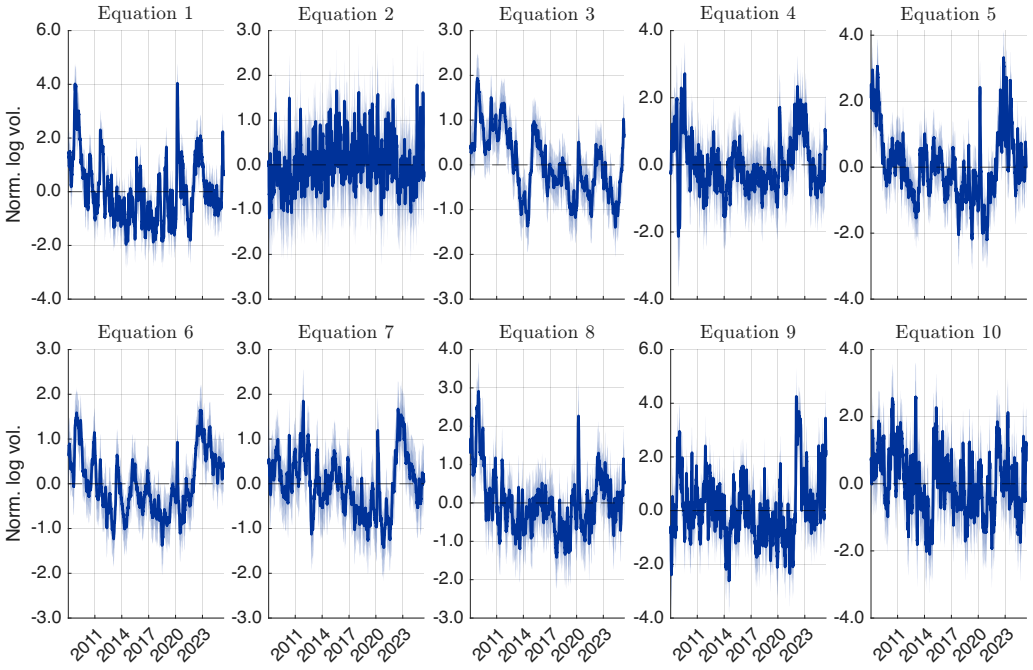
where $\rho_{i,n,t}$ is the forward premium required to hedge currency i into dollars. A positive value ($x^{Rf} > 0$) indicates that cash dollar assets are more convenient than foreign synthetic dollar assets, reflecting the non-pecuniary services—liquidity, collateral value, reserve-currency status—that investors derive from holding dollar-denominated safe assets, consistent with the theoretical mechanism in Bianchi, Bigio, and Engel (2025), where banks' precautionary demand for dollar liquidity generates an endogenous convenience yield on the dollar. A negative value indicates the reverse. The series is constructed as the G10 cross-currency median, smoothed with a 13-day trailing moving average, at the ten-year horizon. An important construction detail concerns the post-LIBOR transition: prior to July 2023, the dollar risk-free rate was proxied by LIBOR; following the discontinuation of LIBOR, the series uses SOFR-based rates, following the methodology in Du et al. (2026) to ensure continuity of the benchmark. The series is available from January 2008 and is sourced from the data page of Wenxin Du.

Treasury Convenience (10Y). Treasury Convenience is the government-bond CIP deviation as defined in Du et al. (2018) and Du et al. (2026). It compares the swapped return on foreign government bonds with the yield on U.S. Treasuries at the same maturity:

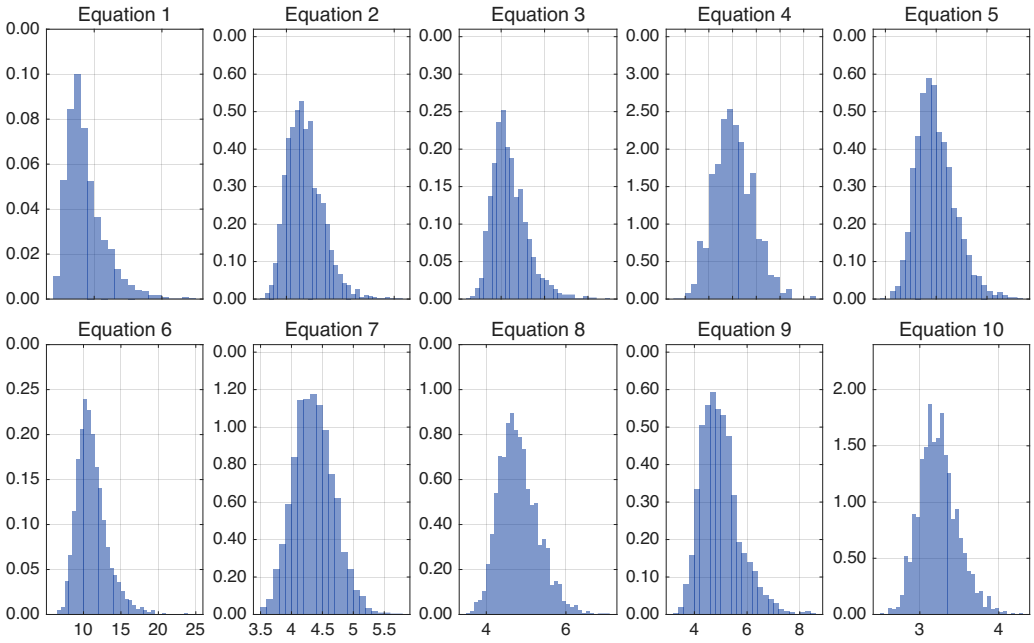
$$x_{i,n,t}^{Govt} = \underbrace{\left(y_{i,n,t}^{Govt} - \rho_{i,n,t}\right)}_{\text{foreign government yield swapped into dollars}} - \underbrace{y_{\$,n,t}^{Govt}}_{\text{U.S. Treasury yield}}$$

A positive value indicates that U.S. Treasuries are more convenient than foreign government bonds; a negative value indicates the reverse. This measure isolates the Treasury-specific component of U.S. safe-asset demand from broader Dollar Convenience. Like Dollar Convenience, it is computed as the G10 median smoothed with a 13-day trailing moving average, and is sourced from the data page of Wenxin Du. Du et al. (2026) show that Dollar Convenience and Treasury Convenience have become increasingly distinct—particularly following the post-crisis restructuring of Treasury markets—making it important to include both measures to separately track changes in global demand for dollar assets from disruptions specific to Treasury-market intermediation.

Figures C.4 and C.5 provide diagnostic evidence relevant to the statistical identification. Figure C.4 reports the estimated stochastic volatility processes together with the posterior distributions of the Student-t degrees-of-freedom parameters, while Figure C.5 reports MCMC trace plots for the normalised impact-matrix coefficients. Together, these diagnostics indicate that the data contain substantial variation in second moments and excess kurtosis, supporting the statistical identification strategy.



(a) Stochastic volatility



(b) Student-t degrees of freedom

Figure C.4: Heteroskedasticity and Non-Gaussianity Metrics

Notes: The figure reports heteroskedasticity metrics from the SV-t model. Panel (a) displays estimated log-volatility for each structural shock. Shaded areas represent 68% and 95% posterior intervals. Panel (b) reports posterior distributions for the degrees-of-freedom parameter ν associated with each shock.

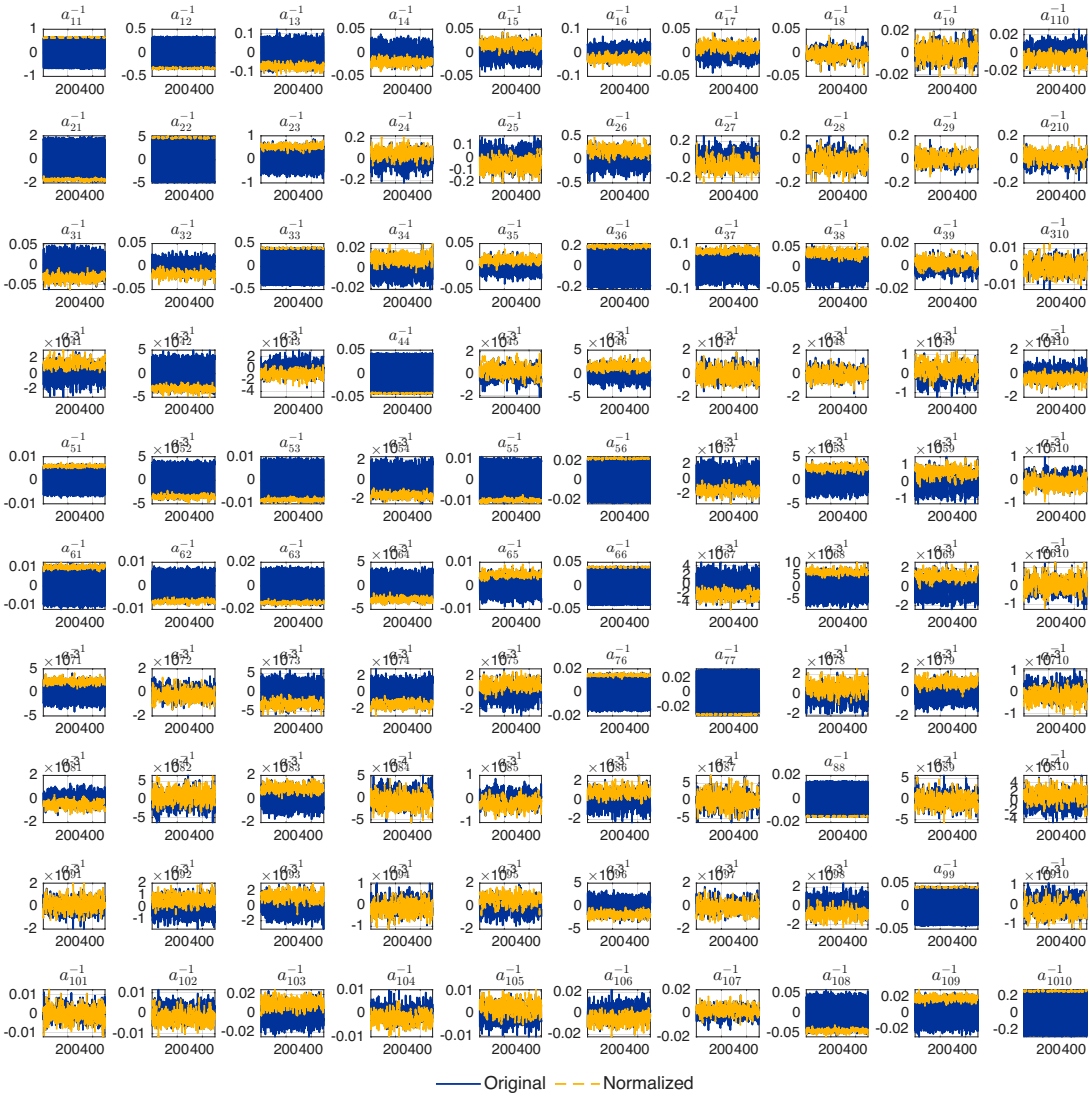


Figure C.5: Posterior draws of the normalised impact matrix

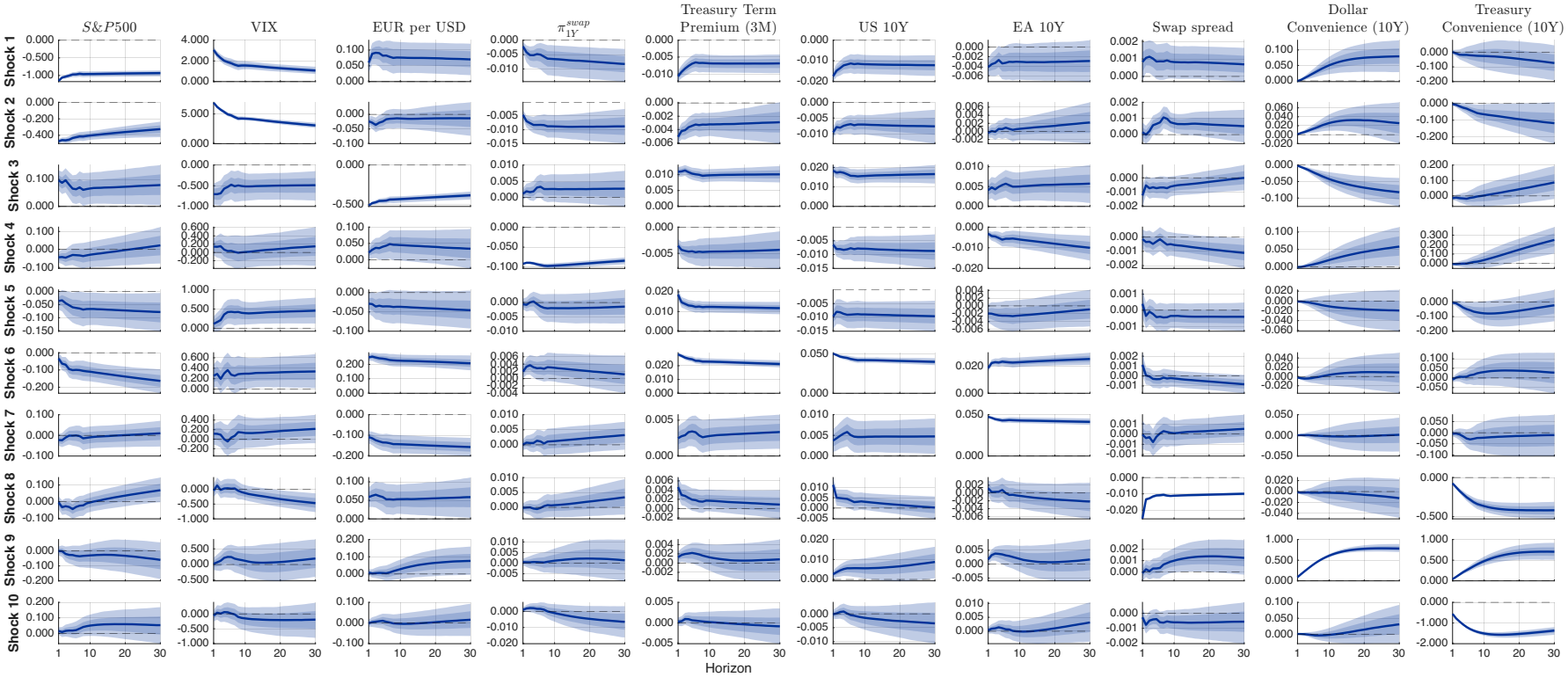
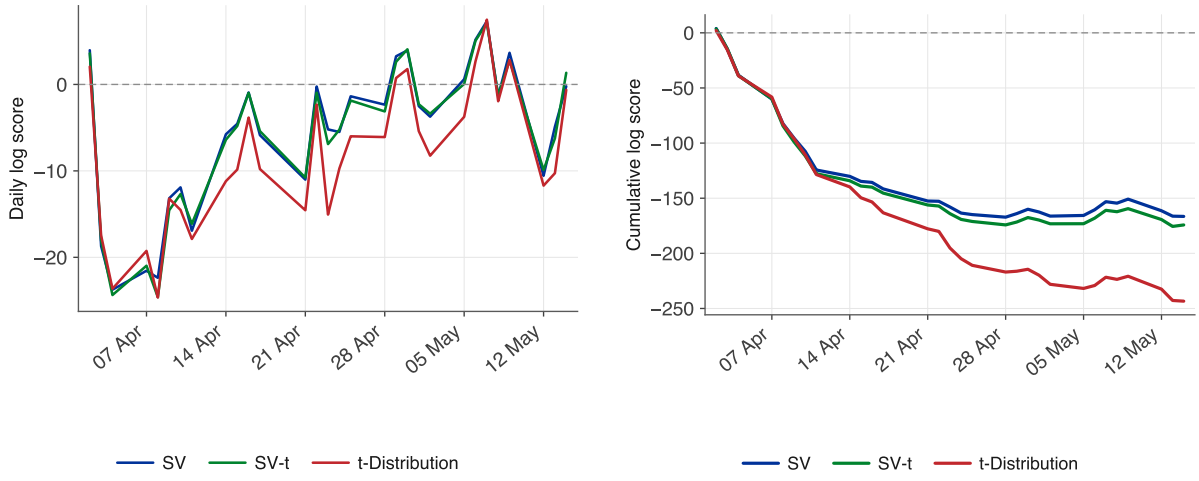


Figure C.6: Impulse response functions to all identified structural shocks

Notes: The figure presents impulse response functions to all ten statistically identified structural shocks over a horizon of 30 days. Shaded areas denote 68% and 95% pointwise posterior intervals.

Model selection. Figure C.7 plots the predictive log scores underlying Table 1: panel (a) reports the daily one-step-ahead log score for each specification over the 2 April–14 May 2025 evaluation window, and panel (b) the corresponding cumulative log score. SV attains the strongest full-sample log score, tracked closely by SV-t throughout the window, while t-Distribution falls visibly and persistently behind from mid-April onward, driving its markedly worse full-sample score despite occasionally matching or exceeding the other two specifications on individual dates. Figures C.8 and C.9 report the impulse responses to the identified shocks under each of the three specifications. SV and SV-t track each other closely throughout, while the t-Distribution specification shows more pronounced quantitative differences in several variables, most visibly for the Safe-Haven and Treasury Market Intermediation shocks. The qualitative signs and relative magnitudes of the responses, and hence the economic interpretation of each shock, are preserved across all three specifications, both for the four shocks discussed in the main text and for the full set of ten statistically identified shocks. Because the three specifications share the same data, variable ordering, and lag structure, we report the shock occupying the same position across all three panels of each figure; as the sign of any individual shock is a normalization choice without economic content (Appendix A.4), we additionally fix each shock's sign relative to our SV-t baseline for visual comparability. These cross-specification comparisons are included as a supplementary robustness illustration; the paper's substantive identification and economic conclusions rely exclusively on the SV-t baseline reported in the main text.



(a) Daily log score

(b) Cumulative log score

Figure C.7: Predictive log scores over time, by variance specification

Notes: Panel (a) reports the daily one-step-ahead predictive log score for each forecast date over the 2 April–14 May 2025 evaluation window used in Table 1; panel (b) reports the corresponding cumulative log score. The SV and SV-t series track each other closely throughout, consistent with their close cumulative and average log scores in Table 1; the t-Distribution series falls visibly and persistently behind from mid-April onward, driving its markedly worse full-sample score despite occasionally matching or exceeding the other two specifications on individual dates.

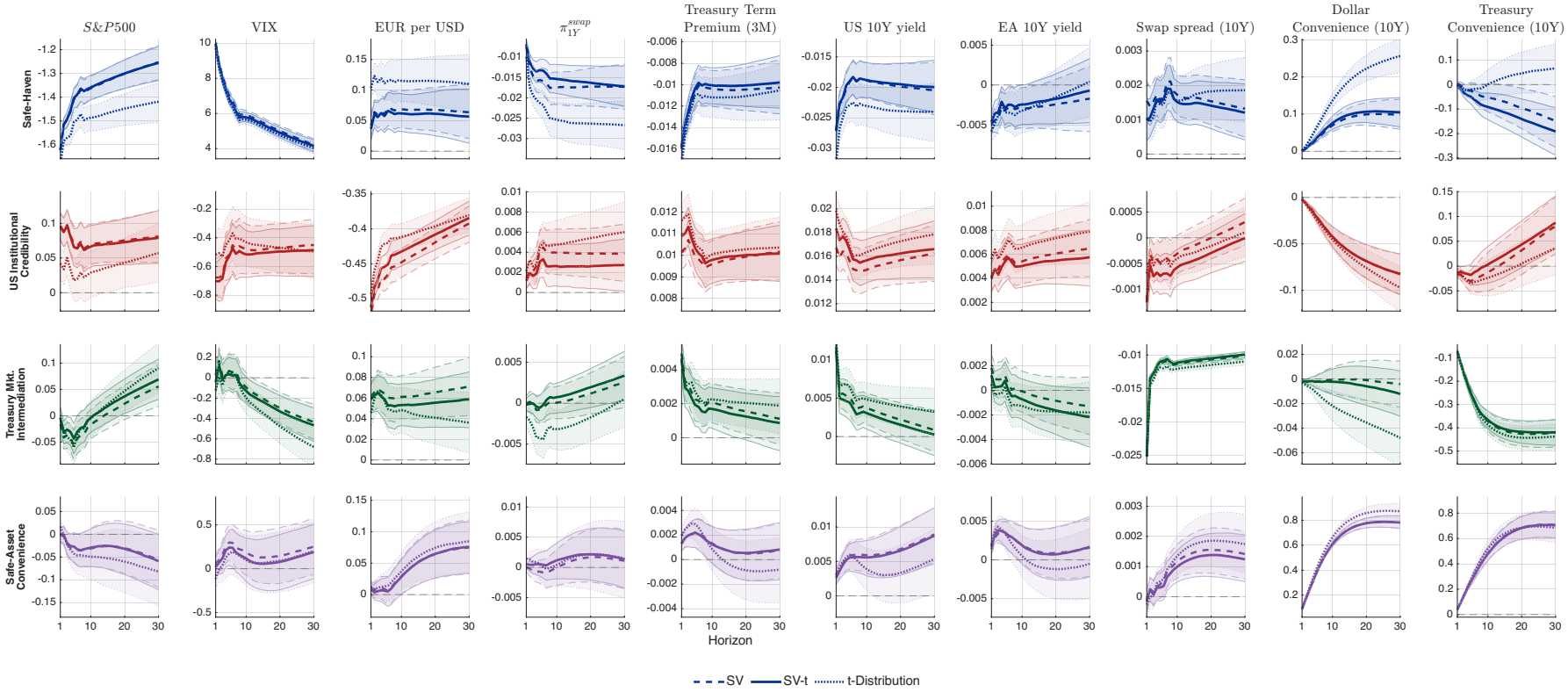


Figure C.8: Impulse response functions across variance specifications: selected shocks

Notes: The figure compares impulse response functions to the four shocks discussed in the main text (*Safe-Haven*, *U.S. Institutional Credibility*, *Treasury Market Intermediation*, and *Safe-Asset Convenience*) across the SV, t-Distribution, and SV-t variance specifications, over a horizon of 30 days. Shaded areas denote 68% pointwise posterior credible intervals.

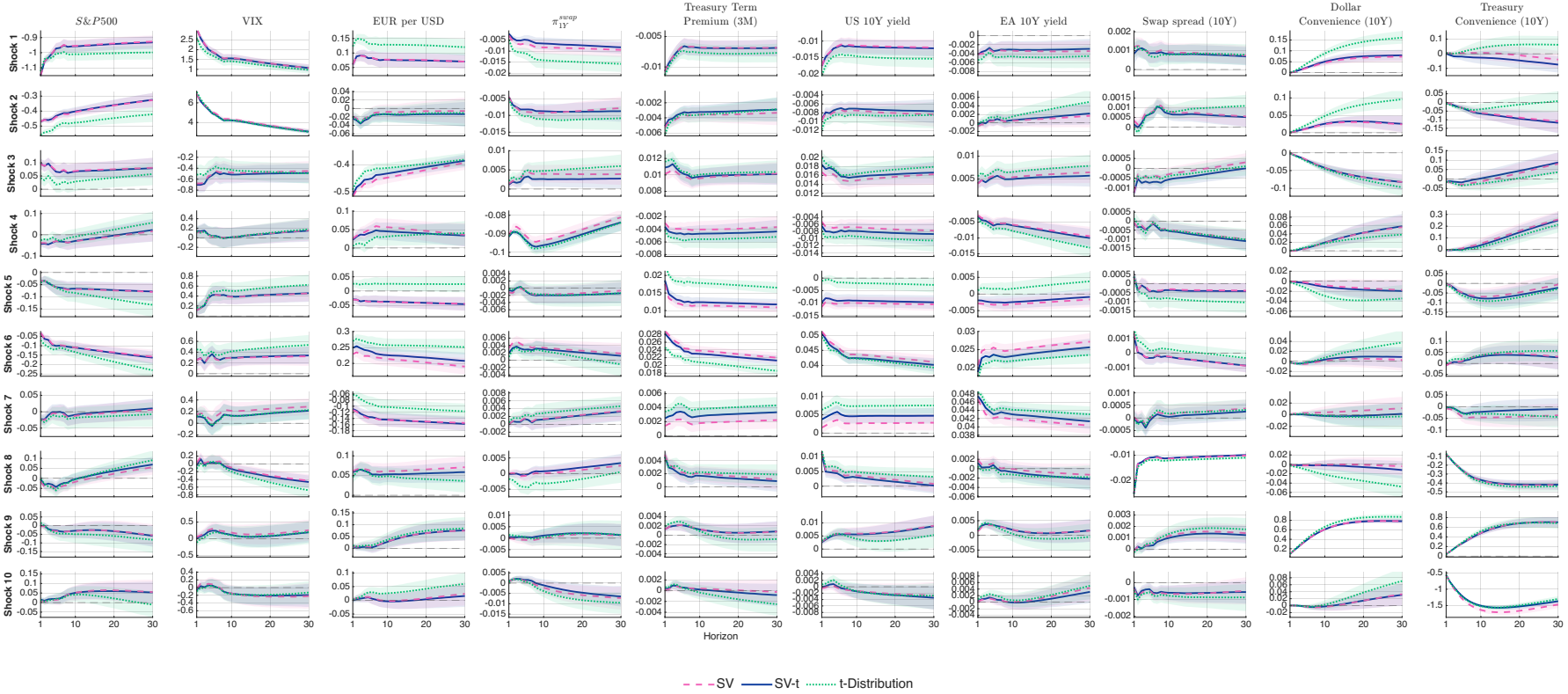
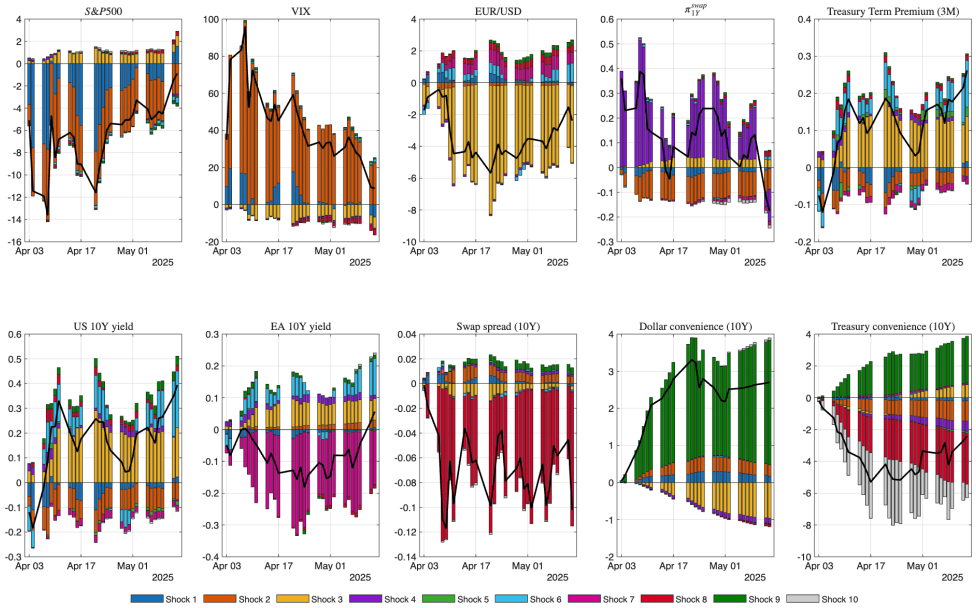
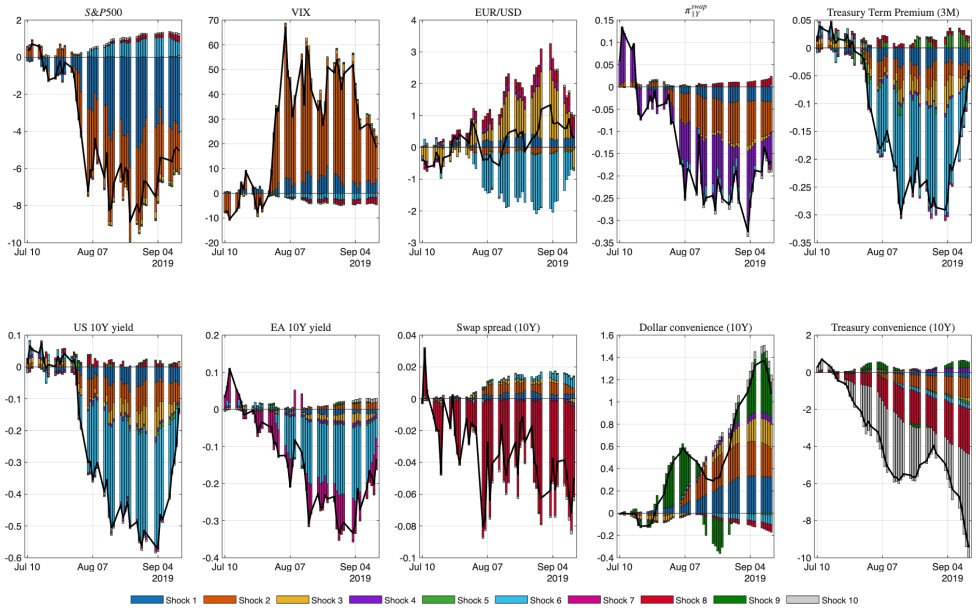


Figure C.9: Impulse response functions across variance specifications: all shocks

Notes: The figure compares impulse response functions to all ten statistically identified structural shocks across the SV, t-Distribution, and SV-t variance specifications, over a horizon of 30 days. Shaded areas denote 68% pointwise posterior credible intervals.



(a) April 2025 tariff announcement



(b) August 2019 tariff escalation

Notes: Panel (a) reports the shock-by-shock historical decomposition for observations from 2 April to 14 May 2025, conditional on the initial observation on 2 April. Panel (b) reports the corresponding decomposition for observations from 9 July to 15 September 2019, conditional on the initial observation on 9 July. Stacked bars show the cumulative contributions of the statistically identified structural shocks; the black line denotes the explained component, measured as the deviation from the deterministic component. *Safe-Haven shock* = shocks 1–2; *U.S. Institutional Credibility shock* = shock 3; *Treasury Market Intermediation shock* = shock 8; *Safe-Asset Convenience shock* = shock 9; Other shocks = shocks 4–7 and 10.

Figure C.10: Shock-by-shock historical decomposition